# Chemical characterization of oxygenated organic compounds in gas-phase and particle-phase using iodide-CIMS with FIGAERO in urban air

Chenshuo Ye[1], Bin Yuan[2,3,*], Yi Lin[2,3], Zelong Wang[2,3], Weiwei Hu[4], Tiange Li[2,3], Wei Chen[4], Caihong Wu[2,3], Chaomin Wang[2,3], Shan Huang[2,3], Jipeng Qi[2,3], Baolin Wang[5], Chen Wang[5], Wei Song[4], Xinming Wang[4], E Zheng[2,3], Jordan E. Krechmer[6], Penglin Ye[7], Zhanyi Zhang[2,3], Xuemei Wang[2,3], Douglas R. Worsnop[6], Min Shao[2,3,1,*]

[1] College of Environmental Sciences and Engineering, Peking University, Beijing 100871, China

[2] Institute for Environmental and Climate Research, Jinan University, Guangzhou 511443, China

[3] Guangdong-Hongkong-Macau Joint Laboratory of Collaborative Innovation for Environmental Quality, Guangzhou 511443, China

[4] Guangzhou Institute of Geochemistry, Chinese Academy of Sciences, Guangzhou 511443, China

[5] School of Environmental Science and Engineering, Qilu University of Technology, Jinan 250353, China

[6] Aerodyne Research, Inc. 45 Manning Rd., Billerica, MA, USA

[7] Shanghai Key Laboratory of Atmospheric Particle Pollution and Prevention (LAP[3]), Department of Environmental Science and Engineering, Fudan University, Shanghai 200438, China

*Correspondence to: byuan@jnu.edu.cn; mshao@pku.edu.cn

## Abstract

The characterization of oxygenated organic compounds in urban areas remains a pivotal gap in our understanding of the evolution of organic carbon under polluted environments, as the atmospheric processes involving interactions between organic and inorganic compounds, anthropogenic pollutants and natural emissions lead to the formation of various and complex secondary products. Here, we describe measurements of an iodide chemical ionization time-of-flight mass spectrometer installed with a Filter Inlet for Gases and AEROsols (FIGAERO-I-CIMS) in both gas-phase and particle-phase at an urban site in Guangzhou, a typical mega-city in southern China, during the autumn of 2018. Abundant oxygenated organic compounds containing 2-5 oxygen atoms were observed, including organic acids, multi-functional organic compounds typically emitted from biomass burning, oxidation products of biogenic hydrocarbons and aromatics. Photochemistry played dominant roles in the formation of gaseous organic acids and isoprene-derived organic nitrates, while nighttime chemistry contributed significantly to the formation of monoterpene-derived organic nitrates and inorganics. Nitrogen-containing organic compounds occupied a significant fraction of the total signal in both the gas and particle phases, with elevated fractions at higher molecular weights. Measurements of organic compounds in particle phase by FIGAERO-I-CIMS explained 24±0.8% of the total organic aerosol mass measured by aerosol mass spectrometer (AMS), and the fraction increased for more aged organic aerosol. The systematical interpretation of mass spectra of the FIGAERO-I-CIMS in the urban area of Guangzhou provides a holistic view of numerous oxygenated organic compounds in the urban atmosphere, which can serve as a reference for the future field measurements by FIGAERO-I-CIMS in polluted urban regions.

# 1 Introduction

In urban air, atmospheric chemical processes are varied and complex, as the result of large emissions of both anthropogenic pollutants and biogenic volatile organic compounds, associated with strong interactions with each other (He et al., 2014; Karl et al., 2018; Shrivastava et al., 2019). Consequently, strong formation of secondary pollutants, e.g. ozone and secondary organic aerosol (SOA), are observed in urban and downwind regions (Huang et al., 2015; Zhang et al., 2014). Oxygenated organic compounds are not fully accounted in some earlier studies, which may explain some of the discrepancies between observations and models for many unaddressed issues in atmospheric chemistry. Oxygenated organic compounds are supposed to be the top candidates for missing OH reactivity observed in various environments including pristine rainforests and urbanized areas (Noelscher et al., 2016; Yang et al., 2016, 2017). The photolysis of carbonyls serves as a critical radical source driving ozone formation in highly polluted industrialized areas (Edwards et al., 2014; Liu et al., 2012; Xue et al., 2016). Although it has been discovered a long time ago that oxygenated organic compounds make up a substantial fraction of submicron aerosol mass (Kroll and Seinfeld, 2008), enormous difficulty still exists in accurately predicting formation and evolution of SOA (de Gouw et al., 2005; Hodzic et al., 2010; Volkamer et al., 2006).

One of the biggest obstacles to understand the role of oxygenated organic compounds is the characterization of these extremely complicated and diverse chemicals which encompass tens of thousands of individual species spanning a wide range of volatility. Chemical ionization mass spectrometry (CIMS) is a powerful technique for the molecular-level characterization of oxygenated organic compounds because of the following advantages (Zhao, 2018): direct measurements and fast time response to capture the rapid temporal change of short-lifetime intermediates; soft ionization providing chemical information on molecular level; selective ionization ensuring measurements for specific classes of species. Iodide anion ionizes species mainly through adduction (Iyer et al., 2016) and is used for the detection of oxygenated organic compounds particularly organic compounds with 2-5 oxygen atoms (Lee et al.,

2014; Lopez-Hilfiker et al., 2016; Riva et al., 2019). It has been shown that I-CIMS is an excellent technique to investigate oxidation processes of volatile organic compounds (VOCs) and formation of SOA (Isaacman-VanWertz et al., 2018). Installed with a thermal desorption inlet that collects and heats aerosol to evaporate organic compounds, e.g. Filter Inlet for Gases and AEROsols (FIGAERO, Lopez-Hilfiker et al., 2014) and Micro Orifice Volatilization Impactor (MOVI-HRToF-CIMS, Yatavelli et al., 2012), the CIMS instruments are capable of analyzing particle-phase species and gas-particle partitioning in a semi-continuous way (Stark et al., 2017; Stolzenburg et al., 2018).

Although FIGAERO-CIMS has gained recent popularity in atmospheric chemistry research, much of the published work was done in chambers or in the laboratory (D'Ambro et al., 2017, 2018; Hammes et al., 2019; Lopez-Hilfiker et al., 2015). As for the applications in field campaigns, most work has been mostly performed in forest or rural areas (Huang et al., 2019; Hunter et al., 2017; Lee et al., 2016, 2018b), and systematic analysis of measurements in urban atmosphere by FIGAERO- CIMS is still limited (Le Breton et al., 2018b). In this study, we present the measurement results using FIGAERO-I-CIMS during a coordinated campaign in Guangzhou, a megacity in the Pearl River Region of China. We provide an overview of gas-phase and particle-phase oxygenated species detected in the mass spectra of FIGAERO-I-CIMS during the campaign. The bulk chemical properties of organic compounds in both gas phase and particle phase will also be discussed.

# 2 Methods

## 2.1 Measurement site and supporting data

Measurements were conducted during the coordinated campaign "Particles, Radicals and Intermediates from oxiDation of primary Emissions over the Great Bay Area" (PRIDE-GBA) in October and November 2018. The Great Bay Area (GBA) refers to a highly industrialized and urbanized area in southern China, including two Special Administrative Regions of Hong Kong and Macao, and nine cities surrounding the Pearl River estuary. Affected by the subtropical monsoon climate, the weather in the region was characterized by high temperatures and relative humidity (RH) as well

as sufficient sunshine (global solar radiation of the Pearl River Delta region in Fall, 2016 was ~1200 MJ/$m^2$, Liu et al., 2018). The city of Guangzhou lies in the north of the GBA and south of the mountains. Therefore, the city is extensively influenced by both anthropogenic and biogenic emissions. The urban site was located at Guangzhou Institute of Geochemistry, Chinese Academy of Sciences (23.14°N, 113.36°E). Online instruments sampled from inlets set up in laboratories on the eighth-floor or ninth-floor (about 25 meters above the ground).

In addition to FIGAERO-I-CIMS discussed later, measurements data from a suite of other instruments were also used in this work. A high-resolution time-of-flight aerosol mass spectrometer (HR-ToF-AMS, Aerodyne Research, Inc.) was deployed to provide chemical composition and many other parameters of ambient aerosol including f60, liquid water content (LWC), particulate organic nitrates and elemental ratios (Hu et al., 2016, 2018). The parameter f60 is the ratio of the integrated signal at m/z 60 to the total signal of organic components and is used as a tracer for biomass burning emissions (Cubison et al., 2011). LWC of aerosol was taken as the sum of water contributed by inorganic components which was predicted by ISORROPIA II model and organic components which was calculated based on the organic hygroscopicity parameter (Fountoukis and Nenes, 2007; Guo et al., 2015). Based on AMS data, organic nitrate concentrations were determined by 2-3 times lower $NO_2^+/NO^+$ ratios for organic nitrate than inorganic nitrate (Fry et al., 2013). The calculation method of elemental ratios based on AMS data has been described elsewhere (Aiken et al., 2007; Canagaratna et al., 2015). Detailed information about AMS measurements from the PRIDE-GBA campaign is forthcoming in a separate manuscript. An online GC-MS/FID (Wuhan Tianhong Instrument Co., Ltd) and a proton transfer reaction time-of-flight mass spectrometer (PTR-ToF-MS, Ionicon Analytic GmbH) (Yuan et al., 2017) served as the analytical techniques for measuring isoprene and other VOCs (e.g. monoterpenes, aromatics and a few oxygenated VOCs) (Wu et al., 2020), respectively. Trace gases (CO, $O_3$, NO and $NO_2$) were measured by commercial gas monitors (Thermo Fisher Scientific Inc.) (Wang et al., 2020d). Photolysis rates were measured by PFS-100 photolysis spectrometer (Focused Photonics Inc.). Temperature and RH were measured

by a Vantage Pro2 weather station (Davis Instruments Corp.). Time series and diurnal profiles of meteorological parameters, trace gases, the photolysis rate of $NO_2$ ($j_{NO_2}$) along with several important VOCs (isoprene, monoterpenes, toluene and benzene) are shown in Figure S1. The temperature during the campaign was between 17 and 33°C with an average of 24°C and RH was between 27 and 97% with an average of 70%.

## 2.2 FIGAERO-I-CIMS

### 2.2.1 Experimental setup

Our instrument consists of a Filter Inlet for Gases and AEROsols (FIGAERO) and a time-of-flight chemical ionization mass spectrometer coupled with an iodide ionization source (Bertram et al., 2011; Lee et al., 2014; Lopez-Hilfiker et al., 2014). The FIGAERO is a multi-port inlet assembly following a two-step procedure alternating between gas mode in which online measurements of gases and semi-continuous sampling of particle-phase species are conducted, and particle mode in which particulate composition is investigated via thermal desorption (Lopez-Hilfiker et al., 2014; Thornton et al., 2020). Iodide source is a "soft" ionization technique with little ionization-induced fragmentation and selective detection towards multi-functional organic compounds, providing elemental compositions for thousands of oxygenated compounds in the atmosphere (Hyttinen et al., 2018; Iyer et al., 2016; Lee et al., 2014; Riva et al., 2019).

The sample air was drawn into the ion molecule reaction (IMR) chamber where it intersected and reacted with the iodide ions generated by flowing 2 mL/min 1000 ppm methyl iodide in 2.4 L/min $N_2$ through an X-ray source. The pressure in the IMR chamber was maintained at 370-390 mbar. Equipped with a long time-of-flight mass analyzer, our instrument was configured to measure singularly charged ions up to 603 Th with a mass resolving power of 10000-11000 (m/Δm at 50% height) during the campaign (Fig. S2).

Ambient air was continuously sampled through two inlets protruding about 1.5 meters out of a window on ninth-floor of a building. One was a 3-meter PFA tubing (1/4-inch OD) for gas phase sampling, through which roughly 9 L/min air was drawn,

and 2 L/min was directly taken into the instrument for gas measurements without removing particles, resulting in an inlet residence time of 0.24 seconds. The gas sampling line inside the room was covered by heat insulation associated with a heating cable to minimize condensation on the tubing surface. The other inlet for particle phase was a 3.8-meter metal tubing (3/8-inch OD) fitted with a $PM_{2.5}$ cyclone and a Nafion dryer (Perma Pure, model PD-07018T-12MSS) to reduce water content in the sampled air. The particle phase inlet was drawn by a laminar flow at ~8 L/min (Reynolds number of ~1500), 3.8 L/min of which was collected on PTFE membrane filters (Zefluor®, Pall Inc., USA). The residence time was 1.3 seconds for the particle phase sampling line. Semi-volatility and low-volatility compounds tend to interact with wall surfaces of both inlet and IMR and thus extend response time (Krechmer et al., 2016). As accurate correction for wall losses remains impossible, no wall loss correction was performed in this study.

The FIGAERO worked in a cyclical 1-hour pattern with two modes (Fig. S3): measuring gas for the first 24 minutes while simultaneously collecting particles on the filter; and then analyzing the particle-phase collection for another 36 minutes. In every 24-minute gas mode, ambient air was measured for the first 21 minutes, followed by 3-minute gas background by overflowing zero air at 5 L/min through a pinhole just in the front of the IMR. The background measurements for CIMS are inevitably influenced by wall interactions, especially for "sticky" species. Recently, Palm et al. (2019) proposed a new way to determine gas background ("fast background") by fast switching between ambient air and background, which greatly improves accurate determination of CIMS background. In the remaining 36 minutes, the components of the collected particles were thermally desorbed and introduced into the CIMS with 2 L/min $N_2$ carrier gas. The $N_2$ flow was ramped from ambient temperature to 175℃ in 12 minutes and held for another 20 minutes. Schematic diagram of working modes and temperature profile of FIGAERO heating in a single cycle is shown in Fig. S4. Particle background was determined every $6^{th}$ 1-hour running cycles in which ambient air passed over a filter (Parker Balston, model 9922-11-CQ) in front of the FIGAERO filter.

### 2.2.2 Calibration experiments

Using various techniques, we calibrated dozens of chemical compounds in the laboratory. Table S1 summarizes the calibrated species and corresponding calibration methods. (1) Gas cylinders are commercially available for a few species (e.g. chlorine, hydrogen cyanide). The gaseous standards were diluted down to different concentrations and then introduced to the CIMS. (2) For those VOCs of which standards are liquid or solid, solutions with known concentrations are made and then vaporized using the liquid calibration unit (LCU, Ionicon Analytic GmbH) to provide gaseous standards. (3) Commercial permeation tubes are available for some species (e.g. nitric acid). (4) Some gaseous chemicals were generated in the laboratory. For example, isocyanic acid was generated from thermal decomposition of cyanuric acid in a diffusion cell (Li et al., 2021; Wang et al., 2020d), and dinitrogen pentoxide was generated via the reaction of ozone with excess nitrogen dioxide in a flow reactor (Bertram et al., 2009). (5) Compounds of low vapor pressure were calibrated through the FIGAERO (Lopez-Hilfiker et al., 2014). Briefly, certain amounts of target species dissolved in organic solvents (e.g. isopropanol or acetone) were deposited onto the PTFE filter of the FIGAERO using a syringe, and the droplet was then subjected to a temperature-programmed thermal desorption by $N_2$ gas. The sensitivity for particle phase was determined as the integrated signals under thermogram profiles versus the amount of deposited calibrant.

In addition to sensitivity calibration, the effects of humidity on the sensitivity for various species were investigated in the laboratory, some of which are shown in Fig. S5. Considering water vapor pressure in the IMR, our humidity-dependent curves are generally consistent with those reported in Lee et al. (2014) (see detailed discussions in Section S3 in the supplement). Low-molecular-weight acids, e.g., formic acid and nitric acid, tend to be more sensitive to the humidity changes than multi-functional compounds. Similar tendency of multi-functional compounds associated with less humidity dependence was also reported in previous work (Lee et al., 2014).

In the later part of the campaign (after Oct. 22), an isotopically labeled formic acid (DCOOH, Cambridge Isotope Laboratories, Inc.) permeation tube held at constant temperature (65 ℃), was mixed with 10 mL/min $N_2$ and continuously delivered into the entrance of sampling inlet in order to derive a humidity dependence function from the field measurements. DCOOH signals during the campaign exhibited a humidity-dependent curve consistent with formic acid obtained in the laboratory (Fig. S5). We applied humidity correction to the species with the humidity-dependent curve determined in the laboratory (underlined species in Table S1). For other compounds, humidity correction was not applied, as there is no universal pattern of humidity dependence for all detected species and multi-functional compounds that comprise the majority of the species measured by FIGAERO-I-CIMS are usually less influenced by humidity.

The measured concentration of DCOOH was steady after being applied to humidity correction (Fig. S6g), indicating the stability of our instrument. In addition, we also performed field calibrations throughout the campaign to check the instrument status by spotting a solution mixture of levoglucosan, heptaethylene glycol and octaethylene glycol on the FIGAERO filter every 2-3 days (Fig. S6). Multiple-point calibrations for these organic species were performed in the beginning and the end of the campaign. The concentration of the solution used in the first two calibration experiments was too high, so we prepared a new solution for calibrations after November. The relative changes of the determined calibration factors in November were within 50% for the calibrated species.

### 2.2.3 Data processing

The TofWare software (version 3.0.3; Tofwerk AG, Switzerland) was used to conduct the high-resolution peak fitting for the mass spectra data of ToF-CIMS, including mass calibration, instrumental parameters optimization (peak shape and peak width) and bunch fitting of high-resolution peaks (Stark et al., 2015). In this study, the signals of ions were normalized to the sum signals of $I^-$ and $H_2OI^-$ at $10^6$ cps. Hourly particle-phase data were obtained by integrating the signals of various ions

during each FIGAERO desorption period. Background corrected signals were obtained by subtracting linearly interpolated background signals from ambient signals (and integrated signals) for ions in the gas (and particle) phase.

In order to determine the sensitivities of uncalibrated species, voltage scanning procedure was performed from time to time throughout the campaign covering different times of the day (Iyer et al., 2016; Lopez-Hilfiker et al., 2016). Here, we selected four representative periods including morning, afternoon, evening and night on polluted days. By performing sigmoidal fitting on the remaining signals as a function of voltages, a $dV_{50}$ value of each ion from each period was determined at which voltage half of one kind of ion dissociated (Lopez-Hilfiker et al., 2016). We observed a positive correlation between the sensitivities of the ions relative to maximum sensitivity and their average $dV_{50}$ values (Fig. S7), consistent with previous studies (Isaacman-VanWertz et al., 2018; Lopez-Hilfiker et al., 2016). This relationship was used to calculate response factors for uncalibrated species, after taking into account the relative transmission efficiency for the ions (see Section S1 in the Supplement for detailed analysis).

# 3 Results and discussion

## 3.1 Overview of detected species in the mass spectra

We identify 1334 ions adducted with iodide from the mass spectra, among which 427 are charged closed-shell organic compounds containing only C, H, O elements ($C_xH_yO_zI^-$) and 388 are charged closed-shell organic compounds containing C, H, O and N elements ($C_xH_yN_{1,2}O_zI^-$). For species with the formula of $C_xH_yO_z$, $x$ ranges from 1 to 20; $y$ is an even number and no more than 2x+2; $z$ is greater than or equal to 2. The range of carbon number $x$ for the ions with $C_xH_yN_{1,2}O_z$ is the same as the ions with $C_xH_yO_z$. For species containing one nitrogen ($C_xH_yNO_z$), $y$ is an odd number and less than 2$x$+2; $z$ is larger than or equal to 2. For species containing two nitrogen atoms ($C_xH_yN_2O_z$), $y$ is an even number and less than 2$x$+1; $z$ is larger than or equal to 4. Table 1 summarizes species discussed in the main text. Although Iodide clusters with two nitrogen atoms and zero nitrogen atoms both lie on odd masses, they can be

separated for certain ions with the current resolving power, as demonstrated by the peak fitting results of mass spectrum at m/z 311 (Fig. S8).

The campaign-averaged mass spectra of detected ions in the both gas and particle phases are shown in Fig. 1. In general, molecules in particle-phase have larger molecular weights compared to gas-phase compounds. Signals in the mass range of 150 - 300 Th comprise a large fraction of gas-phase compounds, and concentrations in the gas phase decrease quickly with m/z higher than 250 Th. In contrast, the detected signals in the particle phase are mainly distributed within the range of 200-320 Th.

We compare the concentration for various ions between the daytime (10 am - 6 pm) and nighttime (10 pm - 6 am), by determining concentration ratios between at night and during the daytime (Fig. 2). Most species have higher concentrations during the daytime, especially for relatively volatile compounds in gas-phase, despite the fact that lower boundary layer height at night should increase nighttime mixing ratios, as behaved for many primary gases, e.g. CO (Fig. S1) (Wu et al., 2020). The higher concentrations during the daytime for most species detected by FIGAERO-I-CIMS suggest the dominant role of photochemical induced oxidation in forming these oxidized compounds. In addition to typical nocturnal species including nitryl chloride ($ClNO_2I^-$), chlorine nitrate ($ClONO_2I^-$) and dinitrogen pentoxide ($N_2O_5I^-$), higher concentrations for the ions of $C_6H_{10}O_5I^-$ and $C_6H_{12}O_5I^-$ were also observed, which will be discussed in next section. A large number of particulate N-containing organic compounds increase during the night as well, as shown by mass defect diagrams of $C_xH_yO_z$ and $C_xH_yN_{1,2}O_z$ color coded by the night to day ratios (Fig. S9).

Based on the mass spectra shown in Fig. 1, we identify a number of ions associated with high concentrations in both gas and particle phases. In the following Section 3.2-3.7, we will perform interpretation of the mass spectra by analyzing variability and correlation of these important ions, including monosaccharide-derived compounds (with brown tags in Fig. 1), oxygenated aromatics (with purple tags), organic acids (with pink tags), oxidation products of biogenic volatile organic compounds (BVOCs, with green tags), sulfur-containing compounds, and inorganics (with blue tags). After going through detailed analysis in the species level, Section 3.8

will provide an overall picture about bulk chemical characteristics of detected organic compounds in terms of the distributions of average carbon oxidation states, carbon number and oxygen number. Lastly, Section 3.9 will compare our measurement of organic aerosol (OA) with AMS data.

## 3.2 Monosaccharide-derived compounds

$C_6H_{10}O_5$ and $C_6H_{12}O_5$ are highly correlated with each other in aerosol (r=0.92), and they are two of a few $C_xH_yO_z$ compounds with higher concentrations at night. Previous work assigned them as monosaccharide derived compounds emitted from biomass burning (Bhattarai et al., 2019; Qi et al., 2019; Reyes-Villegas et al., 2018; Simoneit et al., 1999).

In this campaign, $C_6H_{10}O_5$ was detected mostly in the particle phase (the fraction in the particle phase $F_p$=0.81±0.09) with an average concentration of 0.073±0.076 μg/m$^3$. Its diurnal profile started increasing during dusk, reaching a peak at about midnight and then fell off, as shown in Fig. 3. The mass fraction of $C_6H_{10}O_5$ in OA had a similar diurnal profile, and the ratios of $C_6H_{10}O_5$ to CO increased at night (from 0.17±0.02 to 0.5±0.03 μg·m$^{-3}$/ppm, Fig. 3c), both suggesting enhanced emissions of this compound were related with combustion activities during the evening, e.g., residential biofuel burning for cooking as reported by some previous measurements in China (Wang et al., 2020c; Zhang et al., 2015). Furthermore, the time variations of particle-phase $C_6H_{10}O_5I^-$ were very similar to that of the m/z 60 fragment in AMS mass spectra(Fig. 3a), which is an identified tracer of biomass burning OA produced from the decomposition of levoglucosan and similar compounds during detection by AMS (Brege et al., 2018; Cubison et al., 2011; Schneider et al., 2006). Therefore, $C_6H_{10}O_5$ was probably levoglucosan and its isomers (mannosan and galactosan), and $C_6H_{12}O_5$ was a similar monosaccharide compound emitted from biomass burning.

## 3.3 Oxygenated aromatic compounds

Combustion activities emit a great deal of compounds besides saccharides that the I-CIMS instrument can detect including nitro-aromatics and guaiacol derivatives (Gaston et al., 2016; Kong et al., 2021). Nitro-benzenediols ($C_6H_5NO_4I^-$) as well as

the highly correlated homologue methyl nitro-benzenediols ($C_7H_7NO_4I^-$) (r=0.88 in the particle phase), exhibited double peaks in their diurnal profiles (Fig. 4). Concentrations of $C_6H_5NO_4$ and $C_7H_7NO_4$ were enhanced in the evening, similar to levoglucosan ($C_6H_{10}O_5$). Another concentration peak at noon was also observed for $C_6H_5NO_4$ and $C_7H_7NO_4$. The scatterplot of $C_6H_5NO_4$ as the function of $C_6H_{10}O_5$ exhibits two different slopes (Fig. 5): the lower slope at night (0.088±0.005) indicates the contribution of biomass burning, while the higher slope during the daytime (0.26±0.02) suggests there were other important sources for nitro-aromatics, potentially secondary formation from photooxidation of aromatics (Jenkin et al., 2003). Guaiacol derivatives may have similar sources with nitro-aromatics, as implied by the resemblance of the scatterplots of these two chemical classes versus levoglucosan (cf., Fig. S10 and Fig. 5).

Nitrophenols ($C_6H_5NO_3I^-$), methyl nitrophenols ($C_7H_7NO_3I^-$) and dinitrophenols ($C_6H_4N_2O_5I^-$) were the most significant components of nitro-aromatics in the gas phase. Despite the fact that nitrated phenols could be formed by photochemical oxidation from their aromatic hydrocarbon precursors (Wang et al., 2020a; Yuan et al., 2016), none of them peaked in the daytime, consistent with photolysis as a dominant chemical loss for these compounds (Chen et al., 2011; Yuan et al., 2016). Nitrophenols and methyl nitrophenols peaked in the evening, suggesting either $NO_3$ oxidation or primary emissions was important sources. It is interesting to observe that the peak concentration for $C_6H_4N_2O_5$ was later than the nitrophenols, in agreement with dinitrophenols as the oxidation products from nitrophenols (Harrison et al., 2005).

Several ions identified as oxidation products of aromatics, including $C_7H_6O_4I^-$, $C_7H_8O_4I^-$ and $C_7H_8O_5I^-$ (Mehra et al., 2020; Schwantes et al., 2017), were detected during the campaign. $C_7H_6O_4$ and $C_7H_8O_4$ correlated well with each other (r=0.72). High concentrations of $C_7H_6O_4$ and $C_7H_8O_4$ were mainly observed during the periods with lower $NO_X$ concentration, which was a contrast to the variations of nitrophenols (Fig. S10). We observed the concentration ratios of $C_7H_8O_4I^-$ and $C_7H_7NO_3I^-$ were lower for higher $NO_X$ concentrations (Fig. 5), consistent with the literature that

formation of $C_7H_6O_4$ and $C_7H_8O_4$ is suppressed at high $NO_X$ concentrations (Schwantes et al., 2017). $C_7H_8O_5$ was reported as the ring-retaining oxidation product of $C_7H_8O_4$ which is a typical oxidation product of toluene and cresol (Schwantes et al., 2017; Wang et al., 2020b), as well as the ring-scission products of aromatic hydrocarbons with more carbon atoms, e.g. trimethyl benzenes (Mehra et al., 2020). Given that $C_7H_8O_5$ closely followed with $C_7H_8O_4$ (r=0.93 in particles), toluene oxidation was probably the main contributor to this ion.

## 3.4 Organic acids and related compounds

Organic acids were one of the most abundant species classes detected by I-CIMS (Fig. 1). Low-molecular-weight organic acids (e.g., formic, acetic, glycolic and pyruvic acid) constituted a significant fraction of signals in the mass spectra detected from gas phase. As shown in Fig. 6 (and also Fig. S11), they had very similar temporal trends with diurnal maxima in the afternoon, indicating photochemical oxidation played a dominant role in their formation (de Gouw et al., 2018; Yuan et al., 2015).

In contrast to monocarboxylic acids, dicarboxylic acids partitioned mostly to particle-phase. As the dominant dicarboxylic acids in aerosol (Kawamura and Bikkina, 2016; Mellouki et al., 2015), 94±5% and 74±13% (mean ± one standard deviation of $F_p$) of $C_2H_2O_4$ and $C_3H_4O_4$, assigned as oxalic and malonic acid, were found in particle-phase, respectively. The concentrations of $C_4H_6O_4$ were significantly lower compared to that of C2 and C3 homologous series, but $C_5H_8O_4$ and $C_6H_{10}O_4$ had unexpected higher abundance (Fig. 7). $C_5H_8O_4$ and $C_6H_{10}O_4$ had considerable fractions in the gas phase (45±13% and 43±11%), significantly higher than their C2-C3 homologous series. These two compounds were correlated well with each other in temporal variations (r=0.97 and 0.91 in the gas and particle phases, respectively), and their diurnal variations were different from those of oxalic and malonic acid (Fig. 6). Therefore, dicarboxylic acids may not be the dominant contributing species for the two ions. $C_5H_8O_4$ and $C_6H_{10}O_4$ have been observed from previous study on isoprene oxidation (Berndt et al., 2018, 2019), attributing them as epoxy hydroperoxyl carbonyl and

accretion product, respectively. However, the relative contributions from these possibilities remain unclear.

In addition to the series of $C_nH_{2n-2}O_4$ (i.e. $C_2H_2O_4$, $C_3H_4O_4$), we also observed comparable concentrations of $C_nH_{2n-4}O_4$ ions, especially for carbon number of 4 and 5 ($C_4H_4O_4$ and $C_5H_6O_4$). Considering the double bonds in the molecules, $C_nH_{2n-4}O_4$ should be more reactive than $C_nH_{2n-2}O_4$, suggesting there were large sources for these compounds. Previous studies have reported photo-oxidation of aromatics can generate $C_nH_{2n-4}O_4$, including $C_4H_4O_4$ and $C_5H_6O_4$ (Brege et al., 2018; Kawamura et al., 1996; Kawamura and Bikkina, 2016). Our measurements showed that temporal trends of $C_4H_4O_4$ and $C_5H_6O_4$ followed well with those of aromatic hydrocarbons (Fig. S11b), and thus oxidation of aromatics could be an important contributor to $C_nH_{2n-4}O_4$ in the urban air.

## 3.5 Oxidation products of Biogenic VOCs (BVOCs)

In addition to high anthropogenic emissions of aromatics, terrestrial vegetations nearby also released significant amounts of BVOCs (Wu et al., 2020). During the campaign, the concentrations of isoprene at noon were between 0.1 and 1.5 ppb, whereas the range of daily maxima of monoterpenes was 0.05-2.5 ppb. Hence, a number of oxidation products of BVOCs were detected (Fig. 8 and Fig. S12).

The ion $C_4H_7NO_5I^-$ was the most abundant N-containing C4 organic compounds that were detected in the gas phase. Its daily maxima occurred in the afternoon and correlated moderately with methyl vinyl ketone (MVK) + methacrolein (MACR) measured by PTR-ToF-MS (Fig. 8). We consequently assigned $C_4H_7NO_5$ as MVK nitrates and MACR nitrates, which was reported as the second generation of organic nitrates formed from the oxidation of isoprene hydroxynitrates by OH in the presence of NOx (Fisher et al., 2016; Paulot et al., 2009). Strong correlations were observed between $C_5H_9NO_4I^-$, $C_5H_9NO_5I^-$ and $C_4H_7NO_5I^-$ (r=0.93 and 0.80, respectively), which was in accordance with their similar formation pathways (Jacobs et al., 2014; Wennberg et al., 2018; Xiong et al., 2015). Hence, we expect these three compounds are common oxidation products of isoprene in the polluted atmosphere.

While in aerosol, 2-methylglyceric acid ($C_4H_8O_4$) is a commonly reported oxidation product of isoprene formed in high-$NO_X$ conditions (Surratt et al., 2010). We observed the corresponding ion $C_4H_8O_4I^-$ contributing to OA especially in dry conditions with strong sunlight (Fig. S13). This evidence indicates that isoprene oxidation may contribute to $C_4H_8O_4$, but potential contribution from other sources cannot be ruled out in urban areas.

In terms of monoterpenes, a reasonable correlation (Fig. S14a, r=0.63) was found between the ions $C_{10}H_{16}O_3I^-$ and $C_{10}H_{16}O_2H^+$ measured by PTR-ToF-MS. $C_{10}H_{16}O_2H^+$ was attributed to pinonaldehyde formed from the oxidation of monoterpenes (Glasius et al., 2000; Larsen et al., 2001; Mutzel et al., 2016). Therefore, we tentatively assign $C_{10}H_{16}O_3$ as pinonic acid and its oxocarboxylic acid isomers, which are formed via the oxidation of pinonaldehyde (Fang et al., 2017). $C_8H_{13}NO_6$ also exhibited enhanced gas-phase formation during the day as pinonic acid did. The correlation coefficient of the two compounds (r) was 0.71. In contrast to other monoterpene nitrates, particle-phase $C_8H_{11}NO_7$ and $C_{10}H_{15}NO_6$ peaked at night and decreased during the daytime (Fig. S12), indicative of the role of $NO_3$ in producing organic nitrates as reported in the literature (Faxon et al., 2018). However, $C_{10}H_{15}NO_6I^-$ in the gas phase showed a distinct diurnal profile with peak before the noon. Two possible types of compounds were proposed for $C_{10}H_{15}NO_6$ in previous studies: peroxyacetyl nitrate from pinonaldehyde (Faxon et al., 2018; Nah et al., 2016; Schwantes et al., 2020), or organic nitrates (Bean and Hildebrandt Ruiz, 2016; Boyd et al., 2015). Given the distinct diurnal profiles of $C_{10}H_{15}NO_6I^-$ in the gas and particle phases and the fact that peroxyacetyl nitrate is supposed to dissociate during the FIGAERO heating (Slusher et al., 2004), we speculate that both compounds contributed to this ion. As shown in Fig. S15, $C_8H_{12}O_4$ and $C_9H_{14}O_4$ existed mostly in particle-phase ($F_p$=0.63±0.11 and 0.67±0.10, respectively). We interpreted them as products of monoterpenes via photochemical processes, consistent with the interpretations presented in previous work (Mohr et al., 2013; Mutzel et al., 2015).

## 3.6 S-containing compounds

Organosulfates are concerned as important components of SOA (Hallquist et al., 2009; Surratt et al., 2007), and they can be detected by iodide anion via proton abstraction (Le Breton et al., 2018b; Lee et al., 2014). We detected the ion $C_2H_3SO_6^-$ with peak concentration in the afternoon (Fig. 9). We attributed $C_2H_3SO_6^-$ to glycolic acid sulfate, as suggested by previous work (Galloway et al., 2009; Liao et al., 2015).

Abundant $SO_3I^-$ was detected in particles, and it correlated well with the ion $C_2H_3SO_6^-$ (Fig. 9b) and sulfates measured by AMS (Fig. S16). Previous work observed the sulfite ion radical ($\cdot SO_3^-$) during the ionization of organosulfates (Huang et al., 2018). As a result, the $SO_3I^-$ ion from FIGAERO-I-CIMS might be a potential indicator for the total organosulfates. However, more future work is needed for evaluating this possibility.

Other sulfate-related ions during gas-phase modes were also detected including $HSO_4^-$ (sulfuric acid), $CH_3SO_3^-$ (methanesulfonic acid) which were enhanced in the gas phase during the daytime, in agreement with the notions of photochemically induced gas-phase oxidation (Brandt and van Eldik, 1995). However, these data were not available for quantification given that these low-volatile species would condense on our long gas sampling inlet. It should be noted that measuring sulfuric acid in the gas-phase is difficult and generally requires a "wall-less" source design (Eisele and Tanner, 1993).

## 3.7 Inorganic compounds

There is a growing interest in $N_2O_5$ and its product nitryl chloride ($ClNO_2$) because $ClNO_2$ is found to serve as a nocturnal reservoir of Cl radical and reactive nitrogen, and hence enhance the ozone formation next day (Osthoff et al., 2008; Wang et al., 2016). Time series of $N_2O_5$ and $ClNO_2$ exhibited two patterns. During most of the nights, $N_2O_5$ started to increase quickly at sunset and lasted for only 2-3 hours, and $ClNO_2$ increased in the meantime and ultimately reached its maximum at night, indicative of local formation of $ClNO_2$. However, sometimes a high level of $N_2O_5$ did not lead to an increase in $ClNO_2$ (tinted background in Fig. 10a), probably due to the lack of chloride salts on the aerosol. Other nocturnal species including $ClONO_2$ and $Cl_2$

were highly correlated with $ClNO_2$ as we expected (r=0.92 and 0.83, respectively), suggesting they had common formation mechanisms (Liu et al., 2017).

$HNO_3I^-$ was observed as one of the most abundant species in the mass spectra of FIGAERO-I-CIMS in both gas and particle phase. In the gas phase, the ion $HNO_3I^-$ from I-CIMS has been used to quantify nitric acid (Lee et al., 2018a). The concentrations of gas-phase nitric acid peaked in the afternoon, suggesting photochemistry in the daytime as the dominant source for gas-phase nitric acid.

Previous study suggested that $HNO_3I^-$ from particle-phase measurement by FIGAERO-I-CIMS can be indicative of nitrate in the particle phase (Lee et al., 2016). Here, the concentrations of $HNO_3I^-$ in the particle phase were compared with particulate nitrate measured by AMS (Fig. 11c). Strong correlation was observed (r=0.93), but the concentrations measured by FIGAERO-I-CIMS were higher (slope=1.6), especially for higher concentrations of organic nitrates. Using a threshold of 1 μg/m$^3$ for organic nitrates, the slopes and correlations were higher for the data points with particulate organic nitrates larger than 1 μg/m$^3$ (slope=1.8, r=0.94) than those with less than 1 μg/m$^3$ of organic nitrates (slope=1.1, r=0.90). In short, our measurements suggest that $HNO_3I^-$ in the particle phase from FIGAERO-I-CIMS are formed from thermal-decomposition of both inorganic nitrates (e.g. $NH_4NO_3$) and organic nitrates.

## 3.8 Bulk chemical properties of detected organic compounds

The above discussions on individual chemical groups provide insights into the identification of the mass spectra from FIGAERO-I-CIMS, along with sources and chemistry of oxygenated organic compounds in the urban atmosphere. In this section and the following one, we will provide a bulk analysis of the detected organic compounds.

The composition of organic compounds detected by FIGAERO-I-CIMS was comprehensively characterized with detailed elementary composition in $\overline{OS_C} - n_C$ space (Fig. 12) which depicts the average oxidation states of carbon for closed-shell $C_xH_yO_z$ and $C_xH_yN_{1,2}O_z$ compounds clustered with iodide as a function of carbon

number. The details in calculation of $\overline{OS_C}$ can be found in Section S2 in SI. S-containing compounds were omitted given their negligible variety and concentration compared to the former two chemical classes ($C_xH_yO_z$ and $C_xH_yN_{1,2}O_z$). The average $\overline{OS_C}$ in the particle phase was higher than that in the gas phase at the same carbon number, especially for carbon number between 2 and 10. This agrees with our expectation that more oxidized compounds would partition more strongly in aerosol, as indicated by larger fractions in particles (Fp) for higher $\overline{OS_C}$. In addition, the average $\overline{OS_C}$ generally increased for lower carbon number, as a result of functionalization and fragmentation during VOCs aging. However, there was a notable exception in C5 which had a significantly reduced $\overline{OS_C}$, probably as the result of emissions of isoprene. The analysis of the $\overline{OS_C} - n_C$ space indicates that the large number of organic compounds measured by FIGAERO-I-CIMS are useful to characterize the evolution of organic compounds in the atmosphere.

The distributions of carbon number and oxygen number in the organic compounds measured by FIGAERO-I-CIMS were also investigated, as shown in Fig. 13. Most abundant organic compounds measured by FIGAERO-I-CIMS were C2-C3 compounds, which accounted for about 66% of organic compounds in gas-phase and 56% in particle-phase. It is unexpected that C2-C3 compounds made up such a significant portion of the particle phase, indicating a non-negligible role of thermal decomposition from low volatility compounds such as accretion products or extremely low volatile organic compounds which were reported from FIGAERO measurements on SOA (D'Ambro et al., 2018; Lopez-Hilfiker et al., 2014; Stark et al., 2017). Organic compounds with carbon numbers over 5 constituted only 3% in the gas phase, while they accounted for 30% in the particle phase. The majority of gaseous organic compounds were associated with no more than 3 oxygen atoms. Organic compounds containing 23 oxygen atoms had the largest contribution in both gas-phase (96%) and particle-phase (56%). $C_xH_yN_{1,2}O_z$ accounted for less than 10% of the total oxygenated organic compounds. In the gas phase, compounds with 5-6 oxygen atoms accounted for 51% of $C_xH_yN_{1,2}O_z$, indicative of the high levels of organic nitrates in the urban

atmosphere. Nitrophenols also contributed significantly to $C_xH_yN_{1,2}O_z$ compounds, as they accounted for 74% of $C_xH_yN_{1,2}O_z$ containing 3 oxygen atoms, which in turn contributed to 22% of $C_xH_yN_{1,2}O_z$. In contrast, in the particle phase, the oxygen number of $C_xH_yN_{1,2}O_z$ distributed relatively evenly, as the fractions of compounds with 3-8 oxygen atoms were similar (between 12% and 19%). Compared to measurements in a forest in the southeastern United States (cf., Table S1 from Lee et al., 2016), the fractions of N-containing organic compounds with less than 5 oxygen atoms were significantly larger in our measurements as a result of higher concentrations of nitro-aromatics.

We further determine the fractions of N-containing organic compounds in total organic compounds as a function of m/z. It is clear that the observed fractions of N-containing organic compounds are higher for elevated m/z (Fig. 14) and N-containing ions commonly dominate at even nominal masses (Fig. S17). The gas-phase CHON ions within the m/z range from 250 to 350 Th accounted for about half of the organic compounds in this range. The fractions of CHON ions in particle-phase are somewhat smaller than those in the gas phase for m/z of 250-350 Th, but are comparable for higher m/z. A possible explanation for this is that functional groups of nitrate and nitro reduce less in vapor pressure for organic compounds than functional groups of carboxylic acid or oxygen-equivalent hydroxyl that without nitrogen atom (Capouet and Müller, 2006; Nannoolal et al., 2008; Pankow and Asher, 2008). Consequently, CHON compounds are generally more volatile than CHO compounds with similar molecular weights.

In the end, we determined the total concentration of N-containing organic compounds in the particle-phase measured by FIGAERO-I-CIMS and compared it with the particulate organic nitrates derived from AMS (Fig. 15). Good agreement was achieved when the concentrations of inorganic nitrate were relatively lower, e.g. below 8 μg/m$^3$. However, the discrepancies increased when inorganic nitrate were higher, which can affect the determination of organic nitrate from AMS. This encouraging result indicates that FIGAERO-I-CIMS is able to capture the variability of organic nitrates in the urban atmosphere, which can be helpful in understanding the sources and formation mechanism of these organic nitrates.

## 3.9 Organic aerosol measurements

The total concentrations of organic compounds in the particle phase measured by FIGAERO-I-CIMS were determined and compared with measurements of OA by AMS. The total organic compounds measured by FIGAERO-I-CIMS explained 24±0.8% (fitted slope ± one standard deviation) of the total OA in average (Fig. 16a), which is lower than the average fractions (~50%) reported previously in boreal and temperate forests (Lopez-Hilfiker et al., 2016; Stark et al., 2017). The lower fractions determined here might be as the result of larger contributions to OA from primary emissions in urban air, which are composed of large number of compounds with little signal in I-CIMS (Zhao et al., 2016). As shown in Fig. 16a, organic compounds measured by FIGAERO-I-CIMS account for higher fractions in OA concentrations by AMS for more aged OA, which is consistent with the fact that I-CIMS are more sensitive to oxygenated organic compounds with multiple functional groups (Lee et al., 2014; Lopez-Hilfiker et al., 2016). Furthermore, we expect this fraction to change with the relative contributions of primary emissions and secondary formation for organic compounds in the atmosphere. Similar trends were found in Le Breton et al. (2019), in which an acetate source was used. Acetate ions have been reported to selectively ionize highly oxygenated organic compounds as an iodide source does (Aljawhary et al., 2013).

Comparison of the Van Krevelen diagram between FIGAERO-I-CIMS and AMS also provides useful insights on the measurement of organic compounds in OA. The Van Krevelen diagram has been used as a tool for analyzing functional groups and OA aging by plotting H/C ratios versus O/C ratios (Heald et al., 2010; Lambe et al., 2012). As shown in Fig. 16a, the data points for bulk OA from FIGAERO-I-CIMS follow the same trend as the data points from AMS. However, the bulk OA measured by FIGAERO-I-CIMS only occupied a much smaller region with the O/C ratio between 0.7 and 1.0. We further plot all of the organic compounds in the H/C versus O/C space color-coded with their campaign-average concentrations (Fig. S18a). We observe most particle-phase concentrations measured by FIGAERO-I-CIMS distributed across the zone between the slope of 0 and -1.0. These observations provide additional evidence

that FIGAERO-I-CIMS may only measure the more oxidized organic compounds in OA.

The correlation coefficients between the particle-phase concentrations at unit masses by FIGAERO-I-CIMS and OA mass concentration by AMS are calculated (Fig. S18b). The correlation coefficients are small for ions below m/z 200, as these ions contribute little to organic aerosol. Moderate and strong correlations ($r>0.7$) were observed for the ions between m/z 200 and m/z 400, implying that organic compounds with molecular weight of 100-300 g/mol may account for significant fractions in organic aerosol. The possible reason for the lower correlations of heavier compounds (m/z >400) with OA mass loadings is that these compounds might be related to specific sources or certain chemical processes, which might not contribute at large fractions to the total OA concentration.

## 4 Summary

We deployed a FIGAERO-I-CIMS instrument to measure oxygenated organic compounds in both gas phase and particle phase at a representative urban site in China. The mass spectra measured by FIGAERO-I-CIMS was systematically interpreted. We detected high concentrations of several monosaccharide species (e.g., levoglucosan) potentially emitted from biomass burning, which also contributed to the enhancement of multiple nitro-aromatic species. Photochemistry was also identified as a strong source of nitro-aromatics. Low-molecular-weight organic acids were mainly observed in the gas phase, and observations support daytime photochemistry as the dominant source. Different diurnal profiles for various BVOC-derived organic nitrates were observed, reflecting their different formation pathways related to $NO_X$ chemistry (i.e. daytime photo-oxidation, nocturnal $NO_3$ reactions). Local formation of nitryl chloride was observed, highlighting the potential importance of nighttime chemistry in the urban region.

Our measurements show that oxygenated organic compounds dominated the majority of detected species by FIGAERO-I-CIMS, in which CHO and CHON compounds both accounted for significant fractions. Nitrogen-containing organic

compounds occupied a significant fraction of the total signals in both the gas and particle phases, with elevated fractions at higher molecular weights. The most abundant organic compounds were formic acid and multifunctional organic compounds containing 3-5 oxygen atoms. Organic compounds containing 2 or 3 carbon atoms accounted for over half of the total organic compounds in both gas- and particle phase measured by FIGAERO-I-CIMS. During the campaign, the FIGAERO-I-CIMS measurements explained 24±0.8% of OA measured by AMS, but the fractions are higher for measurements of more aged organic aerosol in the urban atmosphere. This evidence, along with the analysis of the Van Krevelen plot, indicate that FIGAERO-I-CIMS were measuring the more oxidized fraction of OA in the urban air.

## Acknowledgement

This work was supported by the National Key R&D Plan of China (grant No. 2019YFE0106300, 2018YFC0213904, 2016YFC0202206), the National Natural Science Foundation of China (grant No. 41877302), Guangdong Natural Science Funds for Distinguished Young Scholar (grant No. 2018B030306037), Guangdong Provincial Key R&D Plan (grant No. 2019B110206001), Guangdong Soft Science Research Program (grant No. 2019B101001005) and Guangdong Innovative and Entrepreneurial Research Team Program (grant No. 2016ZT06N263). This work was also supported by Special Fund Project for Science and Technology Innovation Strategy of Guangdong Province (Grant No.2019B121205004). Weiwei Hu and Wei Chen were supported by National Natural Science Foundation of China (41875156).

## Data availability

The more detailed data can be provided by contacting the corresponding authors.

## Author contributions

BY and MS designed the research. CSY, YL, ZLW, TGL, WWH, WC, CHW, CMW, SH, JPQ, BLW, CW, WS, XMW, ZYZ, XMW contributed to data collection.

CSY performed the data analysis with contributions from WWH and WC. CSY and BY prepared the manuscript with contributions from JEK and other authors. All the authors reviewed the manuscript.

## Competing interest

The authors declare that they have no conflicts of interest.

## References


Aiken, A. C., DeCarlo, P. F. and Jimenez, J. L.: Elemental Analysis of Organic Species with Electron Ionization High-Resolution Mass Spectrometry, Anal. Chem., 79(21), 8350–8358, doi:10.1021/ac071150w, 2007.

Aljawhary, D., Lee, A. K. Y. and Abbatt, J. P. D.: High-resolution chemical ionization mass spectrometry (ToF-CIMS): Application to study SOA composition and processing, Atmos. Meas. Tech., 6(11), 3211–3224, doi:10.5194/amt-6-3211-2013, 2013.

Bean, J. K. and Hildebrandt Ruiz, L.: Gas-particle partitioning and hydrolysis of organic nitrates formed from the oxidation of alpha-pinene in environmental chamber experiments, Atmos. Chem. Phys., 16(4), 2175–2184, doi:10.5194/acp-16-2175-2016, 2016.

Berndt, T., Scholz, W., Mentler, B., Fischer, L., Herrmann, H., Kulmala, M. and Hansel, A.: Accretion Product Formation from Self- and Cross-Reactions of RO2 Radicals in the Atmosphere, Angew. Chemie Int. Ed., 57(14), 3820–3824, doi:10.1002/anie.201710989, 2018.

Berndt, T., Hyttinen, N., Herrmann, H. and Hansel, A.: First oxidation products from the reaction of hydroxyl radicals with isoprene for pristine environmental conditions, Commun. Chem., 2(1), 1–10, doi:10.1038/s42004-019-0120-9, 2019.

Bertram, T. H., Thornton, J. A. and Riedel, T. P.: An experimental technique for the

684 direct measurement of N2O5 reactivity on ambient particles, Atmos. Meas. Tech.,
685 2(1), 231–242, doi:10.5194/amt-2-231-2009, 2009.
686 Bertram, T. H., Kimmel, J. R., Crisp, T. A., Ryder, O. S., Yatavelli, R. L. N.,
687 Thornton, J. A., Cubison, M. J., Gonin, M. and Worsnop, D. R.: A field-deployable,
688 chemical ionization time-of-flight mass spectrometer, Atmos. Meas. Tech., 4(7),
689 1471–1479, doi:10.5194/amt-4-1471-2011, 2011.
690 Bhattarai, H., Saikawa, E., Wan, X., Zhu, H., Ram, K., Gao, S., Kang, S., Zhang, Q.,
691 Zhang, Y., Wu, G., Wang, X., Kawamura, K., Fu, P. and Cong, Z.: Levoglucosan as a
692 tracer of biomass burning: Recent progress and perspectives, Atmos. Res.,
693 220(November 2018), 20–33, doi:10.1016/j.atmosres.2019.01.004, 2019.
694 Boyd, C. M., Sanchez, J., Xu, L., Eugene, A. J., Nah, T., Tuet, W. Y., Guzman, M. I.
695 and Ng, N. L.: Secondary organic aerosol formation from the β-pinene+NO3 system:
696 effect of humidity and peroxy radical fate, Atmos. Chem. Phys., 15(13), 7497–7522,
697 doi:10.5194/acp-15-7497-2015, 2015.
698 Brandt, C. and van Eldik, R.: Transition Metal-Catalyzed Oxidation of Sulfur(IV)
699 Oxides. Atmospheric-Relevant Processes and Mechanisms, Chem. Rev., 95(1), 119–
700 190, doi:10.1021/cr00033a006, 1995.
701 Brege, M., Paglione, M., Gilardoni, S., Decesari, S., Cristina Facchini, M. and
702 Mazzoleni, L. R.: Molecular insights on aging and aqueous-phase processing from
703 ambient biomass burning emissions-influenced Po Valley fog and aerosol, Atmos.
704 Chem. Phys., 18(17), 13197–13214, doi:10.5194/acp-18-13197-2018, 2018.
705 Le Breton, M., Hallquist, A. M., Pathak, R. K., Simpson, D., Wang, Y., Johansson, J.,
706 Zheng, J., Yang, Y., Shang, D., Wang, H., Liu, Q., Chan, C., Wang, T., Bannan, T. J.,
707 Priestley, M., Percival, C. J., Shallcross, D. E., Lu, K., Guo, S., Hu, M. and Hallquist,
708 M.: Chlorine oxidation of VOCs at a semi-rural site in Beijing: significant chlorine
709 liberation from ClNO2 and subsequent gas- and particle-phase Cl-VOC production,
710 Atmos. Chem. Phys., 18(17), 13013–13030, doi:10.5194/acp-18-13013-2018, 2018a.
711 Le Breton, M., Wang, Y., Hallquist, Å. M., Pathak, R. K., Zheng, J., Yang, Y., Shang,
712 D., Glasius, M., Bannan, T. J., Liu, Q., Chan, C. K., Percival, C. J., Zhu, W., Lou, S.,
713 Topping, D., Wang, Y., Yu, J., Lu, K., Guo, S., Hu, M. and Hallquist, M.: Online gas-

714 and particle-phase measurements of organosulfates, organosulfonates and nitrooxy
715 organosulfates in Beijing utilizing a FIGAERO ToF-CIMS, Atmos. Chem. Phys.,
716 18(14), 10355–10371, doi:10.5194/acp-18-10355-2018, 2018b.
717 Le Breton, M., Psichoudaki, M., Hallquist, M., Watne, Å. K., Lutz, A. and Hallquist,
718 Å. M.: Application of a FIGAERO ToF CIMS for on-line characterization of real-
719 world fresh and aged particle emissions from buses, Aerosol Sci. Technol., 53(3),
720 244–259, doi:10.1080/02786826.2019.1566592, 2019.
721 Canagaratna, M. R., Jimenez, J. L., Kroll, J. H., Chen, Q., Kessler, S. H., Massoli, P.
722 and Ruiz, L. H.: Elemental ratio measurements of organic compounds using aerosol
723 mass spectrometry: characterization, improved calibration, and implications, Atmos.
724 Chem. Phys., 15, 253–272, doi:10.5194/acp-15-253-2015, 2015.
725 Capouet, M. and Müller, J. F.: A group contribution method for estimating the vapour
726 pressures of α-pinene oxidation products, Atmos. Chem. Phys., 6(6), 1455–1467,
727 doi:10.5194/acp-6-1455-2006, 2006.
728 Carlton, A. G., Turpin, B. J., Altieri, K. E., Seitzinger, S., Reff, A., Lim, H.-J. and
729 Ervens, B.: Atmospheric oxalic acid and SOA production from glyoxal: Results of
730 aqueous photooxidation experiments, Atmos. Environ., 41(35), 7588–7602,
731 doi:10.1016/j.atmosenv.2007.05.035, 2007.
732 Carslaw, N.: A mechanistic study of limonene oxidation products and pathways
733 following cleaning activities, Atmos. Environ., 80, 507–513,
734 doi:https://doi.org/10.1016/j.atmosenv.2013.08.034, 2013.
735 Chen, H. and Finlayson-Pitts, B. J.: New Particle Formation from Methanesulfonic
736 Acid and Amines/Ammonia as a Function of Temperature, Environ. Sci. Technol.,
737 51(1), 243–252, doi:10.1021/acs.est.6b04173, 2017.
738 Chen, J., Wenger, J. C. and Venables, D. S.: Near-Ultraviolet Absorption Cross
739 Sections of Nitrophenols and Their Potential Influence on Tropospheric Oxidation
740 Capacity, J. Phys. Chem. A, 115(44), 12235–12242, doi:10.1021/jp206929r, 2011.
741 Cubison, M. J., Ortega, A. M., Hayes, P. L., Farmer, D. K., Day, D., Lechner, M. J.,
742 Brune, W. H., Apel, E., Diskin, G. S., Fisher, J. A., Fuelberg, H. E., Hecobian, A.,
743 Knapp, D. J., Mikoviny, T., Riemer, D., Sachse, G. W., Sessions, W., Weber, R. J.,

744 Weinheimer, A. J., Wisthaler, A. and Jimenez, J. L.: Effects of aging on organic
745 aerosol from open biomass burning smoke in aircraft and laboratory studies, Atmos.
746 Chem. Phys., 11(23), 12049–12064, doi:10.5194/acp-11-12049-2011, 2011.
747 D'Ambro, E. L., Lee, B. H., Liu, J., Shilling, J. E., Gaston, C. J., Lopez-Hilfiker, F.
748 D., Schobesberger, S., Zaveri, R. A., Mohr, C., Lutz, A., Zhang, Z., Gold, A., Surratt,
749 J. D., Rivera-Rios, J. C., Keutsch, F. N. and Thornton, J. A.: Molecular composition
750 and volatility of isoprene photochemical oxidation secondary organic aerosol under
751 low- and high-NOx conditions, Atmos. Chem. Phys., 17(1), 159–174,
752 doi:10.5194/acp-17-159-2017, 2017.
753 D'Ambro, E. L., Schobesberger, S., Zaveri, R. A., Shilling, J. E., Lee, B. H., Lopez-
754 Hilfiker, F. D., Mohr, C. and Thornton, J.: Isothermal evaporation of α-pinene
755 ozonolysis SOA: volatility, phase state, and oligomeric composition, ACS Earth Sp.
756 Chem., acsearthspacechem.8b00084, doi:10.1021/acsearthspacechem.8b00084, 2018.
757 Edwards, P. M., Brown, S. S., Roberts, J. M., Ahmadov, R., Banta, R. M., DeGouw,
758 J. A., Dubé, W. P., Field, R. A., Flynn, J. H., Gilman, J. B., Graus, M., Helmig, D.,
759 Koss, A., Langford, A. O., Lefer, B. L., Lerner, B. M., Li, R., Li, S. M., McKeen, S.
760 A., Murphy, S. M., Parrish, D. D., Senff, C. J., Soltis, J., Stutz, J., Sweeney, C.,
761 Thompson, C. R., Trainer, M. K., Tsai, C., Veres, P. R., Washenfelder, R. A.,
762 Warneke, C., Wild, R. J., Young, C. J., Yuan, B. and Zamora, R.: High winter ozone
763 pollution from carbonyl photolysis in an oil and gas basin, Nature, 514(7522), 351–
764 354, doi:10.1038/nature13767, 2014.
765 Eger, P. G., Schuladen, J., Sobanski, N., Fischer, H., Karu, E., Williams, J., Riva, M.,
766 Zha, Q., Ehn, M., Quéléver, L. L. J., Schallhart, S., Lelieveld, J. and Crowley, J. N.:
767 Pyruvic acid in the boreal forest: gas-phase mixing ratios and impact on radical
768 chemistry, Atmos. Chem. Phys., 20(6), 3697–3711, doi:10.5194/acp-20-3697-2020,
769 2020.
770 Eisele, F. L. and Tanner, D. J.: Measurement of the gas phase concentration of
771 H2SO4 and methane sulfonic acid and estimates of H2SO4 production and loss in the
772 atmosphere, J. Geophys. Res. Atmos., 98(D5), 9001–9010, doi:10.1029/93JD00031,
773 1993.

774 Fang, W., Gong, L. and Sheng, L.: Online analysis of secondary organic aerosols
775 from OH-initiated photooxidation and ozonolysis of α-pinene, β-pinene, Δ3-carene
776 and d-limonene by thermal desorption-photoionisation aerosol mass spectrometry,
777 Environ. Chem., 14(2), 75–90, doi:10.1071/EN16128, 2017.
778 Faxon, C., Hammes, J., Pathak, R. K. and Hallquist, M.: Characterization of organic
779 nitrate constituents of secondary organic aerosol (SOA) from nitrate-radical-initiated
780 oxidation of limonene using High-Resolution Chemical Ionization Mass
781 Spectrometry, Atmos. Chem. Phys., 18, 5467–5481, doi:10.5194/acp-2017-584, 2018.
782 Fisher, J. A., Jacob, D. J., Travis, K. R., Kim, P. S., Marais, E. A., Chan Miller, C.,
783 Yu, K., Zhu, L., Yantosca, R. M. and Sulprizio, M. P.: Organic Nitrate Chemistry and
784 its Implications for Nitrogen Budgets in an Isoprene- and Monoterpene-Rich
785 Atmosphere: Constraints from Aircraft (SEAC4RS) and Ground-Based (SOAS)
786 Observations in the Southeast US, Atmos. Chem. Phys., 16, 5969 [online] Available
787 from: https://www.atmos-chem-phys.net/16/5969/2016/acp-16-5969-2016.pdf, 2016.
788 Fountoukis, C. and Nenes, A.: ISORROPIA II: a computationally efficient
789 thermodynamic equilibrium model for K+–Ca2+–Mg2+–NH+ 4 –Na+–SO2− 4 –NO−
790 3 –Cl−–H2O aerosols, Atmos. Chem. Phys., 7(17), 4639–4659, doi:10.5194/acp-7-
791 4639-2007, 2007.
792 Fry, J. L., Draper, D. C., Zarzana, K. J., Campuzano-Jost, P., Day, D. A., Jimenez, J.
793 L., Brown, S. S., Cohen, R. C., Kaser, L., Hansel, A., Cappellin, L., Karl, T., Hodzic
794 Roux, A., Turnipseed, A., Cantrell, C., Lefer, B. L., Grossberg, N., Farmer, D. K. and
795 Jimenez, J. L.: Observations of gas- and aerosol-phase organic nitrates at BEACHON-
796 RoMBAS 2011, Atmos. Chem. Phys., 13(17), 8585–8605, doi:10.5194/acp-13-8585-
797 2013, 2013.
798 Galloway, M. M., Chhabra, P. S., Chan, A. W. H., Surratt, J. D., Flagan, R. C.,
799 Seinfeld, J. H. and Keutsch, F. N.: Glyoxal uptake on ammonium sulphate seed
800 aerosol: reaction products and reversibility of uptake under dark and irradiated
801 conditions, Atmos. Chem. Phys., 9(10), 3331–3345, doi:10.5194/acp-9-3331-2009,
802 2009.
803 Gaston, C. J., Lopez-Hilfiker, F. D., Whybrew, L. E., Hadley, O., McNair, F., Gao,

804 H., Jaffe, D. A. and Thornton, J. A.: Online molecular characterization of fine
805 particulate matter in Port Angeles, WA: Evidence for a major impact from residential
806 wood smoke, Atmos. Environ., 138, 99–107, doi:10.1016/j.atmosenv.2016.05.013,
807 2016.
808 Glasius, M., Lahaniati, M., Calogirou, A., Di Bella, D., Jensen, N. R., Hjorth, J.,
809 Kotzias, D. and Larsen, B. R.: Carboxylic acids in secondary aerosols from oxidation
810 of cyclic monoterpenes by ozone, Environ. Sci. Technol., 34(6), 1001–1010,
811 doi:10.1021/es990445r, 2000.
812 Gondwe, M., Krol, M., Gieskes, W., Klaassen, W. and de Baar, H.: The contribution
813 of ocean-leaving DMS to the global atmospheric burdens of DMS, MSA, SO2, and
814 NSS SO4=, Global Biogeochem. Cycles, 17(2), doi:10.1029/2002GB001937, 2003.
815 de Gouw, J. A., Middlebrook, A. M., Warneke, C., Goldan, P. D., Kuster, W. C.,
816 Roberts, J. M., Fehsenfeld, F. C., Worsnop, D. R., Canagaratna, M. R., Pszenny, A.
817 A. P., Keene, W. C., Marchewka, M., Bertman, S. B. and Bates, T. S.: Budget of
818 organic carbon in a polluted atmosphere: Results from the New England Air Quality
819 Study in 2002, J. Geophys. Res. D Atmos., 110(16), 1–22,
820 doi:10.1029/2004JD005623, 2005.
821 de Gouw, J. A., Gilman, J. B., Kim, S. W., Alvarez, S. L., Dusanter, S., Graus, M.,
822 Griffith, S. M., Isaacman-VanWertz, G., Kuster, W. C., Lefer, B. L., Lerner, B. M.,
823 McDonald, B. C., Rappenglück, B., Roberts, J. M., Stevens, P. S., Stutz, J., Thalman,
824 R., Veres, P. R., Volkamer, R., Warneke, C., Washenfelder, R. A. and Young, C. J.:
825 Chemistry of Volatile Organic Compounds in the Los Angeles Basin: Formation of
826 Oxygenated Compounds and Determination of Emission Ratios, J. Geophys. Res.
827 Atmos., 123(4), 2298–2319, doi:10.1002/2017JD027976, 2018.
828 Guo, H., Xu, L., Bougiatioti, A., Cerully, K. M., Capps, S. L., Hite, J. R., Carlton, A.
829 G., Lee, S. H., Bergin, M. H., Ng, N. L., Nenes, A. and Weber, R. J.: Fine-particle
830 water and pH in the southeastern United States, Atmos. Chem. Phys., 15(9), 5211–
831 5228, doi:10.5194/acp-15-5211-2015, 2015.
832 Hallquist, M., Wenger, J. C., Baltensperger, U., Rudich, Y., Simpson, D., Claeys, M.,
833 Dommen, J., Donahue, N. M., George, C., Goldstein, a. H., Hamilton, J. F.,

834 Herrmann, H., Hoffmann, T., Iinuma, Y., Jang, M., Jenkin, M. E., Jimenez, J. L.,
835 Kiendler-Scharr, a., Maenhaut, W., McFiggans, G., Mentel, T. F., Monod, a.,
836 Prévôt, a. S. H., Seinfeld, J. H., Surratt, J. D., Szmigielski, R. and Wildt, J.: The
837 formation, properties and impact of secondary organic aerosol: current and emerging
838 issues, Atmos. Chem. Phys., 9(14), 5155–5236, doi:10.5194/acp-9-5155-2009, 2009.
839 Hammes, J., Lutz, A., Mentel, T., Faxon, C. and Hallquist, M.: Carboxylic acids from
840 limonene oxidation by ozone and hydroxyl radicals: insights into mechanisms derived
841 using a FIGAERO-CIMS, Atmos. Chem. Phys., 19(20), 13037–13052,
842 doi:10.5194/acp-19-13037-2019, 2019.
843 Harrison, M. A. J., Barra, S., Borghesi, D., Vione, D., Arsene, C. and Iulian Olariu,
844 R.: Nitrated phenols in the atmosphere: a review, Atmos. Environ., 39(2), 231–248,
845 doi:https://doi.org/10.1016/j.atmosenv.2004.09.044, 2005.
846 He, Q.-F., Ding, X., Wang, X.-M., Yu, J.-Z., Fu, X.-X., Liu, T.-Y., Zhang, Z., Xue, J.,
847 Chen, D.-H., Zhong, L.-J. and Donahue, N. M.: Organosulfates from Pinene and
848 Isoprene over the Pearl River Delta, South China: Seasonal Variation and Implication
849 in Formation Mechanisms, Environ. Sci. Technol., 48(16), 9236–9245,
850 doi:10.1021/es501299v, 2014.
851 Heald, C. L., Kroll, J. H., Jimenez, J. L., Docherty, K. S., Decarlo, P. F., Aiken, A. C.,
852 Chen, Q., Martin, S. T., Farmer, D. K. and Artaxo, P.: A simplified description of the
853 evolution of organic aerosol composition in the atmosphere, Geophys. Res. Lett.,
854 37(8), doi:10.1029/2010GL042737, 2010.
855 Hodzic, A., Jimenez, J. L., Madronich, S., Canagaratna, M. R., Decarlo, P. F.,
856 Kleinman, L. and Fast, J.: Modeling organic aerosols in a megacity: Potential
857 contribution of semi-volatile and intermediate volatility primary organic compounds
858 to secondary organic aerosol formation, Atmos. Chem. Phys., 10(12), 5491–5514,
859 doi:10.5194/acp-10-5491-2010, 2010.
860 Hu, W., Hu, M., Hu, W., Jimenez, J. L., Yuan, B., Chen, W., Wang, M., Wu, Y.,
861 Chen, C., Wang, Z., Peng, J., Zeng, L. and Shao, M.: Chemical composition, sources,
862 and aging process of submicron aerosols in Beijing: Contrast between summer and
863 winter, J. Geophys. Res. Atmos., 121(4), 1955–1977,

doi:10.1002/2015JD024020.Received, 2016.

Hu, W., Day, D. A., Campuzano-Jost, P., Nault, B. A., Park, T., Lee, T., Croteau, P., Canagaratna, M. R., Jayne, J. T., Worsnop, D. R. and Jimenez, J. L.: Evaluation of the new capture vaporizer for aerosol mass spectrometers: Characterization of organic aerosol mass spectra, Aerosol Sci. Technol., 52(7), 725–739, doi:10.1080/02786826.2018.1454584, 2018.

Huang, R.-J., Cao, J., Chen, Y., Yang, L., Shen, J., You, Q., Wang, K., Lin, C., Xu, W., Gao, B., Li, Y., Chen, Q., Hoffmann, T., O'Dowd, C. D., Bilde, M. and Glasius, M.: Organosulfates in atmospheric aerosol: synthesis and quantitative analysis of PM2.5 from Xi'an, northwestern China, Atmos. Meas. Tech., 11(6), 3447–3456, doi:10.5194/amt-11-3447-2018, 2018.

Huang, R. J., Zhang, Y., Bozzetti, C., Ho, K. F., Cao, J. J., Han, Y., Daellenbach, K. R., Slowik, J. G., Platt, S. M., Canonaco, F., Zotter, P., Wolf, R., Pieber, S. M., Bruns, E. A., Crippa, M., Ciarelli, G., Piazzalunga, A., Schwikowski, M., Abbaszade, G., Schnelle-Kreis, J., Zimmermann, R., An, Z., Szidat, S., Baltensperger, U., El Haddad, I. and Prévôt, A. S. H.: High secondary aerosol contribution to particulate pollution during haze events in China, Nature, 514(7521), 218–222, doi:10.1038/nature13774, 2015.

Huang, W., Saathoff, H., Shen, X., Ramisetty, R., Leisner, T. and Mohr, C.: Chemical Characterization of Highly Functionalized Organonitrates Contributing to Night-Time Organic Aerosol Mass Loadings and Particle Growth, Environ. Sci. Technol., 53(3), 1165–1174, doi:10.1021/acs.est.8b05826, 2019.

Hunter, J. F., Day, D. A., Palm, B. B., Yatavelli, R. L. N., Chan, A. W. H., Kaser, L., Cappellin, L., Hayes, P. L., Cross, E. S., Carrasquillo, A. J., Campuzano-Jost, P., Stark, H., Zhao, Y., Hohaus, T., Smith, J. N., Hansel, A., Karl, T., Goldstein, A. H., Guenther, A., Worsnop, D. R., Thornton, J. A., Heald, C. L., Jimenez, J. L. and Kroll, J. H.: Comprehensive characterization of atmospheric organic carbon at a forested site, Nat. Geosci., 10(10), 748–753, doi:10.1038/NGEO3018, 2017.

Hyttinen, N., Otkjær, R. V., Iyer, S., Kjaergaard, H. G., Rissanen, M. P., Wennberg, P. O. and Kurtén, T.: Computational Comparison of Different Reagent Ions in the

Chemical Ionization of Oxidized Multifunctional Compounds, J. Phys. Chem. A, 122(1), 269–279, doi:10.1021/acs.jpca.7b10015, 2018.

Isaacman-VanWertz, G., Massoli, P., O'Brien, R., Lim, C., Franklin, J., Moss, J., Hunter, J., Nowak, J., Canagaratna, M., Misztal, P., Arata, C., Roscioli, J., Herndon, S., Onasch, T., Lambe, A., Jayne, J., Su, L., Knopf, D., Goldstein, A., Worsnop, D. and Kroll, J.: Chemical evolution of atmospheric organic carbon over multiple generations of oxidation, Nat. Chem., 10(4), 462–468, doi:10.1038/s41557-018-0002-2, 2018.

Iyer, S., Lopez-Hilfiker, F., Lee, B. H., Thornton, J. A. and Kurtén, T.: Modeling the Detection of Organic and Inorganic Compounds Using Iodide-Based Chemical Ionization, J. Phys. Chem. A, 120(4), 576–587, doi:10.1021/acs.jpca.5b09837, 2016.

Jacobs, M. I., Burke, W. J. and Elrod, M. J.: Kinetics of the Reactions of Isoprene-Derived Hydroxynitrates: Gas Phase Epoxide Formation and Solution Phase Hydrolysis, Atmos. Chem. Phys., 14, 8933, 2014.

Jenkin, M. E., Saunders, S. M., Wagner, V. and Pilling, M. J.: Protocol for the development of the Master Chemical Mechanism, MCM v3 (Part B): tropospheric degradation of aromatic volatile organic compounds, Atmos. Chem. Phys., 3(1), 181–193, doi:10.5194/acp-3-181-2003, 2003.

Karl, T., Striednig, M., Graus, M., Hammerle, A. and Wohlfahrt, G.: Urban flux measurements reveal a large pool of oxygenated volatile organic compound emissions, Proc. Natl. Acad. Sci., 201714715, doi:10.1073/pnas.1714715115, 2018.

Kawamura, K. and Bikkina, S.: A review of dicarboxylic acids and related compounds in atmospheric aerosols: Molecular distributions, sources and transformation, Atmos. Res., 170, 140–160, doi:https://doi.org/10.1016/j.atmosres.2015.11.018, 2016.

Kawamura, K., Kasukabe, H. and Barrie, L. A.: Source and reaction pathways of dicarboxylic acids, ketoacids and dicarbonyls in arctic aerosols: One year of observations, Atmos. Environ., 30(10), 1709–1722, doi:https://doi.org/10.1016/1352-2310(95)00395-9, 1996.

Kong, X., Salvador, C. M., Carlsson, S., Pathak, R., Davidsson, K. O., Le Breton, M.,

924 Gaita, S. M., Mitra, K., Hallquist, Å. M., Hallquist, M. and Pettersson, J. B. C.:
925 Molecular characterization and optical properties of primary emissions from a
926 residential wood burning boiler, Sci. Total Environ., 754, 142143,
927 doi:https://doi.org/10.1016/j.scitotenv.2020.142143, 2021.
928 Krechmer, J. E., Pagonis, D., Ziemann, P. J. and Jimenez, J. L.: Quantification of Gas-
929 Wall Partitioning in Teflon Environmental Chambers Using Rapid Bursts of Low-
930 Volatility Oxidized Species Generated in Situ, Environ. Sci. Technol., 50(11), 5757–
931 5765, doi:10.1021/acs.est.6b00606, 2016.
932 Kroll, J. H. and Seinfeld, J. H.: Chemistry of secondary organic aerosol: Formation
933 and evolution of low-volatility organics in the atmosphere, Atmos. Environ., 42(16),
934 3593–3624, doi:10.1016/j.atmosenv.2008.01.003, 2008.
935 Lambe, A. T., Onasch, T. B., Croasdale, D. R., Wright, J. P., Martin, A. T., Franklin,
936 J. P., Massoli, P., Kroll, J. H., Canagaratna, M. R., Brune, W. H., Worsnop, D. R. and
937 Davidovits, P.: Transitions from functionalization to fragmentation reactions of
938 laboratory Secondary Organic Aerosol (SOA) generated from the OH oxidation of
939 alkane precursors, Environ. Sci. Technol., 46(10), 5430–5437,
940 doi:10.1021/es300274t, 2012.
941 Larsen, B. R., Di Bella, D., Glasius, M., Winterhalter, R., Jensen, N. R. and Hjorth, J.:
942 Gas-phase OH oxidation of monoterpenes: Gaseous and particulate products, J.
943 Atmos. Chem., 38(3), 231–276, doi:10.1023/A:1006487530903, 2001.
944 Lee, B. H., Lopez-Hilfiker, F. D., Mohr, C., Kurtén, T., Worsnop, D. R. and
945 Thornton, J. A.: An iodide-adduct high-resolution time-of-flight chemical-ionization
946 mass spectrometer: Application to atmospheric inorganic and organic compounds,
947 Environ. Sci. Technol., 48(11), 6309–6317, doi:10.1021/es500362a, 2014.
948 Lee, B. H., Mohr, C., Lopez-Hilfiker, F. D., Lutz, A., Hallquist, M., Lee, L., Romer,
949 P., Cohen, R. C., Iyer, S., Kurtén, T., Hu, W., Day, D. A., Campuzano-Jost, P.,
950 Jimenez, J. L., Xu, L., Ng, N. L., Guo, H., Weber, R. J., Wild, R. J., Brown, S. S.,
951 Koss, A., de Gouw, J., Olson, K., Goldstein, A. H., Seco, R., Kim, S., McAvey, K.,
952 Shepson, P. B., Starn, T., Baumann, K., Edgerton, E. S., Liu, J., Shilling, J. E., Miller,
953 D. O., Brune, W., Schobesberger, S., D'Ambro, E. L. and Thornton, J. A.: Highly

functionalized organic nitrates in the southeast United States: Contribution to secondary organic aerosol and reactive nitrogen budgets, Proc. Natl. Acad. Sci., 113(6), 1516–1521, doi:10.1073/pnas.1508108113, 2016.

Lee, B. H., Lopez-hilfiker, F. D., Veres, P. R., Mcduffie, E. E., Fibiger, D. L., Tamara, L. and Thornton, J. A.: Flight deployment of a high-resolution time-of-flight chemical ionization mass spectrometer : observations of reactive halogen and nitrogen oxide species, , doi:10.1029/2017JD028082, 2018a.

Lee, B. H., Lopez-Hilfiker, F. D., D'Ambro, E. L., Zhou, P., Boy, M., Petäjä, T., Hao, L., Virtanen, A. and Thornton, J. A.: Semi-volatile and highly oxygenated gaseous and particulate organic compounds observed above a boreal forest canopy, Atmos. Chem. Phys., 18(15), 11547–11562, doi:10.5194/acp-18-11547-2018, 2018b.

Li, T., Wang, Z., Yuan, B., Ye, C., Lin, Y., Wang, S., Sha, Q., Yuan, Z., Zheng, J. and Shao, M.: Emissions of carboxylic acids, hydrogen cyanide (HCN) and isocyanic acid (HNCO) from vehicle exhaust, Atmos. Environ., 247, 118218, doi:https://doi.org/10.1016/j.atmosenv.2021.118218, 2021.

Liao, J., Froyd, K. D., Murphy, D. M., Keutsch, F. N., Yu, G., Wennberg, P. O., St Clair, J. M., Crounse, J. D., Wisthaler, A., Mikoviny, T., Jimenez, J. L., Campuzano-Jost, P., Day, D. A., Hu, W., Ryerson, T. B., Pollack, I. B., Peischl, J., Anderson, B. E., Ziemba, L. D., Blake, D. R., Meinardi, S. and Diskin, G.: Airborne measurements of organosulfates over the continental U.S, J. Geophys. Res. Atmos. JGR, 120(7), 2990–3005, doi:10.1002/2014JD022378, 2015.

Lim, H.-J., Carlton, A. G. and Turpin, B. J.: Isoprene Forms Secondary Organic Aerosol through Cloud Processing: Model Simulations, Environ. Sci. Technol., 39(12), 4441–4446, doi:10.1021/es048039h, 2005.

Liu, C., Deng, X., Zhu, B. and Yin, C.: Characteristics of GSR of China's three major economic regions in the past 10 years and its relationship with O3 and PM2.5, China Environ. Sci., 38(08), 2820–2829, doi:10.19674/j.cnki.issn1000-6923.2018.0295, 2018.

Liu, X., Qu, H., Huey, L. G., Wang, Y., Sjostedt, S., Zeng, L., Lu, K., Wu, Y., Hu, M., Shao, M., Zhu, T. and Zhang, Y.: High Levels of Daytime Molecular Chlorine

and Nitryl Chloride at a Rural Site on the North China Plain, Environ. Sci. Technol., 51(17), 9588–9595, doi:10.1021/acs.est.7b03039, 2017.

Liu, Z., Wang, Y., Gu, D., Zhao, C., Huey, L. G., Stickel, R., Liao, J., Shao, M., Zhu, T., Zeng, L., Amoroso, A., Costabile, F., Chang, C. C. and Liu, S. C.: Summertime photochemistry during CAREBeijing-2007: ROxbudgets and O3 formation, Atmos. Chem. Phys., 12(16), 7737–7752, doi:10.5194/acp-12-7737-2012, 2012.

Lopez-Hilfiker, F. D., Mohr, C., Ehn, M., Rubach, F., Kleist, E., Wildt, J., Mentel, T. F., Lutz, A., Hallquist, M., Worsnop, D. and Thornton, J. A.: A novel method for online analysis of gas and particle composition: description and evaluation of a Filter Inlet for Gases and AEROsols (FIGAERO), Atmos. Meas. Tech., 7(4), 983–1001, doi:10.5194/amt-7-983-2014, 2014.

Lopez-Hilfiker, F. D., Mohr, C., Ehn, M., Rubach, F., Kleist, E., Wildt, J., Mentel, T. F. and Carrasquillo, A. J.: Phase partitioning and volatility of secondary organic aerosol components formed from α -pinene ozonolysis and OH oxidation : the importance of accretion products and other low volatility compounds, Atmos. Chem. Phys., 15, 7765–7776, doi:10.5194/acp-15-7765-2015, 2015.

Lopez-Hilfiker, F. D., Iyer, S., Mohr, C., Lee, B. H., Ambro, E. L. D., Kurtén, T. and Thornton, J. A.: Constraining the sensitivity of iodide adduct chemical ionization mass spectrometry to multifunctional organic molecules using the collision limit and thermodynamic stability of iodide ion adducts, Atmos. Meas. Tech., 9, 1505–1512, doi:10.5194/amt-9-1505-2016, 2016.

Massoli, P., Stark, H., Canagaratna, M. R., Krechmer, J. E., Xu, L., Ng, N. L., Mauldin, R. L., Yan, C., Kimmel, J., Misztal, P. K., Jimenez, J. L., Jayne, J. T. and Worsnop, D. R.: Ambient Measurements of Highly Oxidized Gas-Phase Molecules during the Southern Oxidant and Aerosol Study (SOAS) 2013, ACS Earth Sp. Chem., 2(7), 653–672, doi:10.1021/acsearthspacechem.8b00028, 2018.

Mattila, J. M., Brophy, P., Kirkland, J., Hall, S., Ullmann, K., Fischer, E. V., Brown, S., McDuffie, E., Tevlin, A. and Farmer, D. K.: Tropospheric sources and sinks of gas-phase acids in the Colorado Front Range, Atmos. Chem. Phys., 18(16), 12315–12327, doi:10.5194/acp-18-12315-2018, 2018.

Mehra, A., Wang, Y., Krechmer, J. E., Lambe, A., Majluf, F., Morris, M. A., Priestley, M., Bannan, T. J., Bryant, D. J., Pereira, K. L., Hamilton, J. F., Rickard, A. R., Newland, M. J., Stark, H., Croteau, P., Jayne, J. T., Worsnop, D. R., Canagaratna, M. R., Wang, L. and Coe, H.: Evaluation of the chemical composition of gas- and particle-phase products of aromatic oxidation, Atmos. Chem. Phys., 20(16), 9783–9803, doi:10.5194/acp-20-9783-2020, 2020.

Mellouki, A., Wallington, T. J. and Chen, J.: Atmospheric Chemistry of Oxygenated Volatile Organic Compounds: Impacts on Air Quality and Climate, Chem. Rev., 115(10), 3984–4014, doi:10.1021/cr500549n, 2015.

Mohr, C., Lopez-Hilfiker, F. D., Zotter, P., Prévôt, A. S. H., Xu, L., Ng, N. L., Herndon, S. C., Williams, L. R., Franklin, J. P., Zahniser, M. S., Worsnop, D. R., Knighton, W. B., Aiken, A. C., Gorkowski, K. J., Dubey, M. K., Allan, J. D. and Thornton, J. A.: Contribution of Nitrated Phenols to Wood Burning Brown Carbon Light Absorption in Detling, United Kingdom during Winter Time, Environ. Sci. Technol., 47(12), 6316–6324, doi:10.1021/es400683v, 2013.

Mutzel, A., Poulain, L., Berndt, T., Iinuma, Y., Rodigast, M., Böge, O., Richters, S., Spindler, G., Sipila¨, M., Jokinen, T., Kulmala, M. and Herrmann, H.: Highly Oxidized Multifunctional Organic Compounds Observed in Tropospheric Particles: A Field and Laboratory Study, Environ. Sci. Technol., 49(13), 7754–7761, doi:10.1021/acs.est.5b00885, 2015.

Mutzel, A., Rodigast, M., Iinuma, Y., Böge, O. and Herrmann, H.: Monoterpene SOA - Contribution of first-generation oxidation products to formation and chemical composition, Atmos. Environ., 130, 136–144, doi:10.1016/j.atmosenv.2015.10.080, 2016.

Nah, T., Sanchez, J., Boyd, C. M. and Ng, N. L.: Photochemical Aging of α-pinene and β-pinene Secondary Organic Aerosol formed from Nitrate Radical Oxidation, Environ. Sci. Technol., 50(1), 222–231, doi:10.1021/acs.est.5b04594, 2016.

Nannoolal, Y., Rarey, J. and Ramjugernath, D.: Estimation of pure component properties Part 3. Estimation of the vapor pressure of non-electrolyte organic compounds via group contributions and group interactions, Fluid Phase Equilib.,

269(1–2), 117–133, doi:10.1016/j.fluid.2008.04.020, 2008.
Ng, N. L., Brown, S. S., Archibald, A. T., Atlas, E., Cohen, R. C., Crowley, J. N., Day, D. A., Donahue, N. M., Fry, J. L., Fuchs, H., Griffin, R. J., Guzman, M. I., Herrmann, H., Hodzic, A., Iinuma, Y., Jimenez, J. L., Kiendler-Scharr, A., Lee, B. H., Luecken, D. J., Mao, J., McLaren, R., Mutzel, A., Osthoff, H. D., Ouyang, B., Picquet-Varrault, B., Platt, U., Pye, H. O. T., Rudich, Y., Schwantes, R. H., Shiraiwa, M., Stutz, J., Thornton, J. A., Tilgner, A., Williams, B. J. and Zaveri, R. A.: Nitrate radicals and biogenic volatile organic compounds: oxidation, mechanisms, and organic aerosol, Atmos. Chem. Phys., 17(3), 2103–2162, doi:10.5194/acp-17-2103-2017, 2017.
Noelscher, A. C., Yanez-Serrano, A. M., Wolff, S., de Araujo, A. C., Lavric, J. V, Kesselmeier, J. and Williams, J.: Unexpected seasonality in quantity and composition of Amazon rainforest air reactivity, Nat. Commun., 7, doi:10.1038/ncomms10383, 2016.
Osthoff, H. D., Roberts, J. M., Ravishankara, A. R., Williams, E. J., Lerner, B. M., Sommariva, R., Bates, T. S., Coffman, D., Quinn, P. K., Dibb, J. E., Stark, H., Burkholder, J. B., Talukdar, R. K., Meagher, J., Fehsenfeld, F. C. and Brown, S. S.: High levels of nitryl chloride in the polluted subtropical marine boundary layer, Nat. Geosci., 1(5), 324–328, doi:10.1038/ngeo177, 2008.
Palm, B. B., Liu, X., Jimenez, J. L. and Thornton, J. A.: Performance of a new coaxial ion-molecule reaction region for low-pressure chemical ionization mass spectrometry with reduced instrument wall interactions, Atmos. Meas. Tech., 12(11), 5829–5844, doi:10.5194/amt-12-5829-2019, 2019.
Pankow, J. F. and Asher, W. E.: SIMPOL.1: A simple group contribution method for predicting vapor pressures and enthalpies of vaporization of multifunctional organic compounds, Atmos. Chem. Phys., 8(10), 2773–2796, doi:10.5194/acp-8-2773-2008, 2008.
Paulot, F., Crounse, J. D., Kjaergaard, H. G., Kroll, J. H., Seinfeld, J. H. and Wennberg, P. O.: Isoprene photooxidation: New insights into the production of acids and organic nitrates, Atmos. Chem. Phys., 9(4), 1479–1501, doi:10.5194/acp-9-1479-

2009, 2009.
Qi, L., Chen, M., Stefenelli, G., Pospisilova, V., Tong, Y., Bertrand, A., Hueglin, C., Ge, X., Baltensperger, U., Prévôt, A. S. H. and Slowik, J. G.: Organic aerosol source apportionment in Zurich using an extractive electrospray ionization time-of-flight mass spectrometer (EESI-TOF-MS) – Part 2: Biomass burning influences in winter, Atmos. Chem. Phys., 19(12), 8037–8062, doi:10.5194/acp-19-8037-2019, 2019.
Reyes-Villegas, E., Bannan, T., Le Breton, M., Mehra, A., Priestley, M., Percival, C., Coe, H. and Allan, J. D.: Online Chemical Characterization of Food-Cooking Organic Aerosols: Implications for Source Apportionment, Environ. Sci. Technol., 52(9), 5308–5318, doi:10.1021/acs.est.7b06278, 2018.
Riva, M., Rantala, P., Krechmer, J. E., Peräkylä, O., Zhang, Y., Heikkinen, L., Garmash, O., Yan, C., Kulmala, M., Worsnop, D. and Ehn, M.: Evaluating the performance of five different chemical ionization techniques for detecting gaseous oxygenated organic species, Atmos. Meas. Tech., 2018(4), 1–39, doi:10.5194/amt-2018-407, 2019.
Sander, R. and Crutzen, P. J.: Model study indicating halogen activation and ozone destruction in polluted air masses transported to the sea, J. Geophys. Res. Atmos., 101(D4), 9121–9138, doi:10.1029/95JD03793, 1996.
Schneider, J., Weimer, S., Drewnick, F., Borrmann, S., Helas, G., Gwaze, P., Schmid, O., Andreae, M. O. and Kirchner, U.: Mass spectrometric analysis and aerodynamic properties of various types of combustion-related aerosol particles, Int. J. Mass Spectrom., 258(1), 37–49, doi:https://doi.org/10.1016/j.ijms.2006.07.008, 2006.
Schwantes, R. H., Teng, A. P., Nguyen, T. B., Coggon, M. M., Crounse, J. D., St Clair, J. M., Zhang, X., Schilling, K. A., Seinfeld, J. H. and Wennberg, P. O.: Isoprene NO3 Oxidation Products from the RO2 + HO2 Pathway, J. Phys. Chem. A, 119, 10158, 2015.
Schwantes, R. H., Schilling, K. A., McVay, R. C., Lignell, H., Coggon, M. M., Zhang, X., Wennberg, P. O. and Seinfeld, J. H.: Formation of highly oxygenated low-volatility products from cresol oxidation, Atmos. Chem. Phys., 17(5), 3453–3474, doi:10.5194/acp-17-3453-2017, 2017.

Schwantes, R. H., Emmons, L. K., Orlando, J. J., Barth, M. C., Tyndall, G. S., Hall, S. R., Ullmann, K., St. Clair, J. M., Blake, D. R., Wisthaler, A. and Paul V. Bui, T.: Comprehensive isoprene and terpene gas-phase chemistry improves simulated surface ozone in the southeastern US, Atmos. Chem. Phys., 20(6), 3739–3776, doi:10.5194/acp-20-3739-2020, 2020.

Shrivastava, M., Andreae, M. O., Artaxo, P., Barbosa, H. M. J., Berg, L. K., Brito, J., Ching, J., Easter, R. C., Fan, J., Fast, J. D., Feng, Z., Fuentes, J. D., Glasius, M., Goldstein, A. H., Alves, E. G., Gomes, H., Gu, D., Guenther, A., Jathar, S. H., Kim, S., Liu, Y., Lou, S., Martin, S. T., McNeill, V. F., Medeiros, A., de Sá, S. S., Shilling, J. E., Springston, S. R., Souza, R. A. F., Thornton, J. A., Isaacman-VanWertz, G., Yee, L. D., Ynoue, R., Zaveri, R. A., Zelenyuk, A. and Zhao, C.: Urban pollution greatly enhances formation of natural aerosols over the Amazon rainforest, Nat. Commun., 10(1), doi:10.1038/s41467-019-08909-4, 2019.

Simoneit, B. R. T., Schauer, J. J., Nolte, C. G., Oros, D. R., Elias, V. O., Fraser, M. P., Rogge, W. F. and Cass, G. R.: Levoglucosan, a tracer for cellulose in biomass burning and atmospheric particles, Atmos. Environ., 33(2), 173–182, doi:https://doi.org/10.1016/S1352-2310(98)00145-9, 1999.

Slusher, D. L., Huey, L. G., Tanner, D. J., Flocke, F. M. and Roberts, J. M.: A thermal dissociation–chemical ionization mass spectrometry (TD-CIMS) technique for the simultaneous measurement of peroxyacyl nitrates and dinitrogen pentoxide, J. Geophys. Res. Atmos., 109(D19), doi:10.1029/2004JD004670, 2004.

Stark, H., Yatavelli, R. L. N., Thompson, S. L., Kimmel, J. R., Cubison, M. J., Chhabra, P. S., Canagaratna, M. R., Jayne, J. T., Worsnop, D. R. and Jimenez, J. L.: Methods to extract molecular and bulk chemical information from series of complex mass spectra with limited mass resolution, Int. J. Mass Spectrom., 389, 26–38, doi:10.1016/j.ijms.2015.08.011, 2015.

Stark, H., Yatavelli, R. L. N., Thompson, S. L., Kang, H., Krechmer, J. E., Kimmel, J. R., Palm, B. B., Hu, W., Hayes, P. L., Day, D. A., Campuzano-Jost, P., Canagaratna, M. R., Jayne, J. T., Worsnop, D. R. and Jimenez, J. L.: Impact of Thermal Decomposition on Thermal Desorption Instruments: Advantage of Thermogram

Analysis for Quantifying Volatility Distributions of Organic Species, Environ. Sci. Technol., 51(15), 8491–8500, doi:10.1021/acs.est.7b00160, 2017.

Stolzenburg, D., Fischer, L., Vogel, A. L., Heinritzi, M., Schervish, M., Simon, M., Wagner, A. C., Dada, L., Ahonen, L. R., Amorim, A., Baccarini, A., Bauer, P. S., Baumgartner, B., Bergen, A., Bianchi, F., Breitenlechner, M., Brilke, S., Buenrostro Mazon, S., Chen, D., Dias, A., Draper, D. C., Duplissy, J., El Haddad, I., Finkenzeller, H., Frege, C., Fuchs, C., Garmash, O., Gordon, H., He, X., Helm, J., Hofbauer, V., Hoyle, C. R., Kim, C., Kirkby, J., Kontkanen, J., Kürten, A., Lampilahti, J., Lawler, M., Lehtipalo, K., Leiminger, M., Mai, H., Mathot, S., Mentler, B., Molteni, U., Nie, W., Nieminen, T., Nowak, J. B., Ojdanic, A., Onnela, A., Passananti, M., Petäjä, T., Quéléver, L. L. J., Rissanen, M. P., Sarnela, N., Schallhart, S., Tauber, C., Tomé, A., Wagner, R., Wang, M., Weitz, L., Wimmer, D., Xiao, M., Yan, C., Ye, P., Zha, Q., Baltensperger, U., Curtius, J., Dommen, J., Flagan, R. C., Kulmala, M., Smith, J. N., Worsnop, D. R., Hansel, A., Donahue, N. M., Winkler, P. M., Nie, W., Passananti, M., Leiminger, M., Stolzenburg, D., Yan, C., Wimmer, D., Buenrostro Mazon, S., Kontkanen, J., Wang, M., Garmash, O., Kulmala, M., Petäjä, T., Bianchi, F., Chen, D., Nieminen, T., Brilke, S., Nowak, J. B., Duplissy, J., El Haddad, I., Simon, M., Wagner, A. C., Kürten, A., Smith, J. N., Kim, C., et al.: Rapid growth of organic aerosol nanoparticles over a wide tropospheric temperature range, Proc. Natl. Acad. Sci., 115(37), 201807604, doi:10.1073/pnas.1807604115, 2018.

Surratt, J. D., Murphy, S. M., Kroll, J. H., Ng, N. L., Hildebrandt, L., Sorooshian, A., Szmigielski, R., Vermeylen, R., Maenhaut, W., Claeys, M., Flagan, R. C. and Seinfeld, J. H.: Chemical Composition of Secondary Organic Aerosol Formed from the Photooxidation of Isoprene, J. Phys. Chem. A, 110(31), 9665–9690, doi:10.1021/jp061734m, 2006.

Surratt, J. D., Kroll, J. H., Kleindienst, T. E., Edney, E. O., Claeys, M., Sorooshian, A., Ng, N. L., Offenberg, J. H., Lewandowski, M., Jaoui, M., Flagan, R. C. and Seinfeld, J. H.: Evidence for Organosulfates in Secondary Organic Aerosol, Environ. Sci. Technol., 41(2), 517–527, doi:10.1021/es062081q, 2007.

Surratt, J. D., Chan, A. W. H., Eddingsaas, N. C., Chan, M., Loza, C. L., Kwan, A. J., Hersey, S. P., Flagan, R. C., Wennberg, P. O. and Seinfeld, J. H.: Reactive intermediates revealed in secondary organic aerosol formation from isoprene, Proc. Natl. Acad. Sci., 107(15), 6640–6645, doi:10.1073/pnas.0911114107, 2010.

Thornton, J. A., Mohr, C., Schobesberger, S., D'Ambro, E. L., Lee, B. H. and Lopez-Hilfiker, F. D.: Evaluating Organic Aerosol Sources and Evolution with a Combined Molecular Composition and Volatility Framework Using the Filter Inlet for Gases and Aerosols (FIGAERO), Acc. Chem. Res., 53(8), 1415–1426, doi:10.1021/acs.accounts.0c00259, 2020.

Volkamer, R., Jimenez, J. L., San Martini, F., Dzepina, K., Zhang, Q., Salcedo, D., Molina, L. T., Worsnop, D. R. and Molina, M. J.: Secondary organic aerosol formation from anthropogenic air pollution: Rapid and higher than expected, Geophys. Res. Lett., 33(17), doi:10.1029/2006GL026899, 2006.

Wang, H., Gao, Y., Wang, S., Wu, X., Liu, Y., Li, X., Huang, D., Lou, S., Wu, Z., Guo, S., Jing, S., Li, Y., Huang, C., Tyndall, G. S., Orlando, J. J. and Zhang, X.: Atmospheric Processing of Nitrophenols and Nitrocresols from Biomass Burning Emissions, J. Geophys. Res. Atmos., 0–3, doi:10.1029/2020JD033401, 2020a.

Wang, M., Chen, D., Xiao, M., Ye, Q., Stolzenburg, D., Hofbauer, V., Ye, P., Vogel, A. L., Mauldin, R. L., Amorim, A., Baccarini, A., Baumgartner, B., Brilke, S., Dada, L., Dias, A., Duplissy, J., Finkenzeller, H., Garmash, O., He, X.-C., Hoyle, C. R., Kim, C., Kvashnin, A., Lehtipalo, K., Fischer, L., Molteni, U., Petäjä, T., Pospisilova, V., Quéléver, L. L. J., Rissanen, M., Simon, M., Tauber, C., Tomé, A., Wagner, A. C., Weitz, L., Volkamer, R., Winkler, P. M., Kirkby, J., Worsnop, D. R., Kulmala, M., Baltensperger, U., Dommen, J., El-Haddad, I. and Donahue, N. M.: Photo-oxidation of Aromatic Hydrocarbons Produces Low-Volatility Organic Compounds, Environ. Sci. Technol., 54(13), 7911–7921, doi:10.1021/acs.est.0c02100, 2020b.

Wang, Q., He, X., Zhou, M., Huang, D. D., Qiao, L., Zhu, S., Ma, Y., Wang, H., Li, L., Huang, C., Huang, X. H. H., Xu, W., Worsnop, D., Goldstein, A. H., Guo, H. and Yu, J. Z.: Hourly Measurements of Organic Molecular Markers in Urban Shanghai, China: Primary Organic Aerosol Source Identification and Observation of Cooking

Aerosol Aging, ACS Earth Sp. Chem., 4(9), 1670–1685, doi:10.1021/acsearthspacechem.0c00205, 2020c.

Wang, T., Tham, Y. J., Xue, L., Li, Q., Zha, Q., Wang, Z., Poon, S. C. N., Dube, W. P., Blake, D. R., Louie, P. K. K., Luk, C. W. Y., Tsui, W., Brown, S. S., Osthoff, H. D., Roberts, J. M., Ravishankara, A. R., Williams, E. J., Lerner, B. M., Sommariva, R., Bates, T. S., Coffman, D., Quinn, P. K., Dibb, J. E., Stark, H., Burkholder, J. B., Talukdar, R. K., Meagher, J., Fehsenfeld, F. C. and Brown, S. S.: Observations of nitryl chloride and modeling its source and effect on ozone in the planetary boundary layer of southern China, J. Geophys. Res., 121(5), 2476–2489, doi:10.1002/2015JD024556, 2016.

Wang, X., Jacob, D. J., Eastham, S. D., Sulprizio, M. P., Zhu, L., Chen, Q., Alexander, B., Sherwen, T., Evans, M. J., Lee, B. H., Haskins, J. D., Lopez-Hilfiker, F. D., Thornton, J. A., Huey, G. L. and Liao, H.: The role of chlorine in global tropospheric chemistry, Atmos. Chem. Phys., 19(6), 3981–4003, doi:10.5194/acp-19-3981-2019, 2019.

Wang, Z., Yuan, B., Ye, C., Roberts, J., Wisthaler, A., Lin, Y., Li, T., Wu, C., Peng, Y., Wang, C., Wang, S., Yang, S., Wang, B., Qi, J., Wang, C., Song, W., Hu, W., Wang, X., Xu, W., Ma, N., Kuang, Y., Tao, J., Zhang, Z., Su, H., Cheng, Y., Wang, X. and Shao, M.: High Concentrations of Atmospheric Isocyanic Acid (HNCO) Produced from Secondary Sources in China, Environ. Sci. Technol., 11818–11826, doi:10.1021/acs.est.0c02843, 2020d.

Wennberg, P. O., Bates, K. H., Crounse, J. D., Dodson, L. G., McVay, R. C., Mertens, L. A., Nguyen, T. B., Praske, E., Schwantes, R. H., Smarte, M. D., St Clair, J. M., Teng, A. P., Zhang, X. and Seinfeld, J. H.: Gas-Phase Reactions of Isoprene and Its Major Oxidation Products, Chem. Rev., 118(7), 3337–3390, doi:10.1021/acs.chemrev.7b00439, 2018.

Wu, C., Wang, C., Wang, S., Wang, W., Yuan, B., Qi, J., Wang, B., Wang, H., Wang, C., Song, W., Wang, X., Hu, W., Lou, S., Ye, C., Peng, Y., Wang, Z., Huangfu, Y., Xie, Y., Zhu, M., Zheng, J., Wang, X., Jiang, B., Zhang, Z. and Shao, M.: Measurement report: Important contributions of oxygenated compounds to emissions

and chemistry of VOCs in urban air, Atmos. Chem. Phys., 14769–14785, doi:10.5194/acp-2020-152, 2020.

Xiong, F., McAvey, K. M., Pratt, K. A., Groff, C. J., Hostetler, M. A., Lipton, M. A., Starn, T. K., Seeley, J. V, Bertman, S. B. and Teng, A. P.: Observation of Isoprene Hydroxynitrates in the Southeastern United States and Implications for the Fate of NOx, Atmos. Chem. Phys., 15, 11257, 2015.

Xue, L., Gu, R., Wang, T., Wang, X., Saunders, S., Blake, D., Louie, P. K. K., Luk, C. W. Y., Simpson, I., Xu, Z., Wang, Z., Gao, Y., Lee, S., Mellouki, A. and Wang, W.: Oxidative capacity and radical chemistry in the polluted atmosphere of Hong Kong and Pearl River Delta region: analysis of a severe photochemical smog episode, Atmos. Chem. Phys., 16(15), 9891–9903, doi:10.5194/acp-16-9891-2016, 2016.

Yang, Y., Shao, M., Wang, X., Nölscher, A. C., Kessel, S., Guenther, A. and Williams, J.: Towards a quantitative understanding of total OH reactivity: A review, Atmos. Environ., 134(2), 147–161, doi:10.1016/j.atmosenv.2016.03.010, 2016.

Yang, Y., Shao, M., Keßel, S., Li, Y., Lu, K., Lu, S., Williams, J., Zhang, Y., Zeng, L., Nölscher, A. C., Wu, Y., Wang, X. and Zheng, J.: How the OH reactivity affects the ozone production efficiency: case studies in Beijing and Heshan, China, Atmos. Chem. Phys., 17(11), 7127–7142, doi:10.5194/acp-17-7127-2017, 2017.

Yasmeen, F., Szmigielski, R., Vermeylen, R., Gomez-Gonzalez, Y., Surratt, J. D., Chan, A. W. H., Seinfeld, J. H., Maenhaut, W. and Claeys, M.: Mass spectrometric characterization of isomeric terpenoic acids from the oxidation of alpha-pinene, beta-pinene, d-limonene, and Delta(3)-carene in fine forest aerosol, J. MASS Spectrom., 46(4), 425–442, doi:10.1002/jms.1911, 2011.

Yatavelli, R. L. N., Lopez-Hilfiker, F., Wargo, J. D., Kimmel, J. R., Cubison, M. J., Bertram, T. H., Jimenez, J. L., Gonin, M., Worsnop, D. R. and Thornton, J. A.: A Chemical Ionization High-Resolution Time-of-Flight Mass Spectrometer Coupled to a Micro Orifice Volatilization Impactor (MOVI-HRToF-CIMS) for Analysis of Gas and Particle-Phase Organic Species, Aerosol Sci. Technol., 46(12), 1313–1327, doi:10.1080/02786826.2012.712236, 2012.

Yuan, B., Veres, P. R., Warneke, C., Roberts, J. M., Gilman, J. B., Koss, A., Edwards,

P. M., Graus, M., Kuster, W. C., Li, S. M., Wild, R. J., Brown, S. S., Dubé, W. P., Lerner, B. M., Williams, E. J., Johnson, J. E., Quinn, P. K., Bates, T. S., Lefer, B., Hayes, P. L., Jimenez, J. L., Weber, R. J., Zamora, R., Ervens, B., Millet, D. B., Rappenglück, B. and De Gouw, J. A.: Investigation of secondary formation of formic acid: Urban environment vs. oil and gas producing region, Atmos. Chem. Phys., 15(4), 1975–1993, doi:10.5194/acp-15-1975-2015, 2015.

Yuan, B., Liggio, J., Wentzell, J., Li, S. M., Stark, H., Roberts, J. M., Gilman, J., Lerner, B., Warneke, C., Li, R., Leithead, A., Osthoff, H. D., Wild, R., Brown, S. S. and De Gouw, J. A.: Secondary formation of nitrated phenols: Insights from observations during the Uintah Basin Winter Ozone Study (UBWOS) 2014, Atmos. Chem. Phys., 16(4), 2139–2153, doi:10.5194/acp-16-2139-2016, 2016.

Yuan, B., Koss, A. R., Warneke, C., Coggon, M., Sekimoto, K. and De Gouw, J. A.: Proton-Transfer-Reaction Mass Spectrometry: Applications in Atmospheric Sciences, Chem. Rev., 117(21), 13187–13229, doi:10.1021/acs.chemrev.7b00325, 2017.

Zhang, Q., Yuan, B., Shao, M., Wang, X., Lu, S., Lu, K., Wang, M., Chen, L., Chang, C.-C. and Liu, S. C.: Variations of ground-level O3 and its precursors in Beijing in summertime between 2005 and 2011, Atmos. Chem. Phys., 14(12), 6089–6101, doi:10.5194/acp-14-6089-2014, 2014.

Zhang, Y. J., Tang, L. L., Wang, Z., Yu, H. X., Sun, Y. L., Liu, D., Qin, W., Canonaco, F., Prévôt, A. S. H., Zhang, H. L. and Zhou, H. C.: Insights into characteristics, sources, and evolution of submicron aerosols during harvest seasons in the Yangtze River delta region, China, Atmos. Chem. Phys., 15(3), 1331–1349, doi:10.5194/acp-15-1331-2015, 2015.

Zhao, R.: The Recent Development and Application of Chemical Ionization Mass Spectrometry in Atmospheric Chemistry., 2018.

Zhao, Y., Nguyen, N. T., Presto, A. A., Hennigan, C. J., May, A. A. and Robinson, A. L.: Intermediate Volatility Organic Compound Emissions from On-Road Gasoline Vehicles and Small Off-Road Gasoline Engines, Environ. Sci. Technol., 50(8), 4554–4563, doi:10.1021/acs.est.5b06247, 2016.

Zhou, Y., Huang, X. H., Bian, Q., Griffith, S. M., Louie, P. K. K. and Yu, J. Z.:

1284 Sources and atmospheric processes impacting oxalate at a suburban coastal site in
1285 Hong Kong: Insights inferred from 1 year hourly measurements, J. Geophys. Res.
1286 Atmos., 120(18), 9772–9788, doi:10.1002/2015JD023531, 2015.
1287

1288 **Table 1.** The detected ions discussed in the text.

| Ion formula | m/z | Assigned compounds | Possible formation pathways | References |
|---|---|---|---|---|
| $C_6H_{10}O_5I^-$ | 288.96 | Levoglucosan, mannosan and galactosan | Biomass burning or cooking emissions | (Gaston et al., 2016; Reyes-Villegas et al., 2018) |
| $C_6H_{12}O_5I^-$ | 290.97 | Fucose | Biomass burning emissions | (Qi et al., 2019) |
| $C_6H_5NO_3I^-$ | 265.93 | Nitro-phenols | Direct emissions, oxidation of aromatics in the presence of NOx | (Gaston et al., 2016; Yuan et al., 2016) |
| $C_6H_5NO_4I^-$ | 281.93 | Nitro-benzenediols | Direct emissions, oxidation of aromatics in the presence of NOx | (Gaston et al., 2016; Yuan et al., 2016) |
| $C_6H_4N_2O_5I^-$ | 310.92 | Dinitro-phenols | Direct emissions, oxidation of aromatics in the presence of NOx | (Gaston et al., 2016; Yuan et al., 2016) |
| $C_7H_7NO_3I^-$ | 279.95 | Methyl nitro-phenols | Direct emissions, oxidation of aromatics in the presence of NOx | (Gaston et al., 2016; Yuan et al., 2016) |
| $C_7H_7NO_4I^-$ | 295.94 | Methyl nitro-benzenediols | Direct emissions, oxidation of aromatics in the presence of NOx | (Gaston et al., 2016; Yuan et al., 2016) |
| $C_7H_6O_4I^-$ | 280.93 | Dihydroxy methyl benzoquinone | Aromatics + OH | (Schwantes et al., 2017; Wang et al., 2020b) |
| $C_7H_8O_4I^-$ | 282.95 | Tetrahydroxy toluene | Aromatics + OH | (Schwantes et al., 2017; Wang et al., 2020b) |
| $C_7H_8O_5I^-$ | 298.94 | Pentahydroxy toluene, fragments of C9 aromatics | Aromatics + OH | (Mehra et al., 2020; Schwantes et al., 2017) |

| | | | | |
|---|---|---|---|---|
| $CH_2O_2I^-$ | 172.91 | Formic acid | Oxidation of VOCs | (Lee et al., 2014; Yuan et al., 2015) |
| $C_2H_4O_2I^-$ | 186.93 | Acetic acid | Oxidation of VOCs | (Lee et al., 2014; Mattila et al., 2018) |
| $C_5H_{10}O_2I^-$ | 228.97 | Pentanoic acid | Traffic emissions, secondary formation | (Mattila et al., 2018) |
| $C_2H_4O_3I^-$ | 202.92 | Glycolic acid | Oxidation of VOCs | (Lee et al., 2014; Lim et al., 2005) |
| $C_3H_4O_3I^-$ | 214.92 | Pyruvic acid | Photolysis of methylglyoxal, BVOCs+OH, photo-oxidation of aromatics in the presence of $NO_X$ | (Eger et al., 2020; Mattila et al., 2018) |
| $C_2H_2O_4I^-$ | 216.90 | Oxalic acid | Aqueous-phase photooxidation of glyoxal, photo-oxidation of VOCs | (Carlton et al., 2007; Lee et al., 2014; Zhou et al., 2015) |
| $C_3H_4O_4I^-$ | 230.92 | Malonic acid, hydroxypyruvic acid | Oxidation of VOCs | (Kawamura and Bikkina, 2016; Lee et al., 2014) |
| $C_4H_4O_4I^-$ | 242.92 | Maleic acid, fumaric acid | Oxidation of aromatics | (Brege et al., 2018; Kawamura et al., 1996) |
| $C_5H_6O_4I^-$ | 256.93 | Unsaturated dicarboxylic acid | Oxidation of aromatics | (Brege et al., 2018; Kawamura et al., 1996) |
| $C_5H_8O_4I^-$ | 258.95 | | Photo-oxidation of VOCs | (Berndt et al., 2019; Kawamura and Bikkina, 2016) |
| $C_6H_{10}O_4I^-$ | 272.96 | | Photo-oxidation of VOCs | (Berndt et al., 2019; Kawamura and Bikkina, 2016) |

| | | | | |
|---|---|---|---|---|
| $C_4H_8O_4I^-$ | 246.95 | 2-methylglyceric acid | Isoprene SOA component under high $NO_X$ conditions | (Surratt et al., 2006, 2010) |
| $C_5H_9NO_4I^-$ | 273.96 | IHN (isoprene hydroxy nitrates) | 1st-genetration organic nitrates from reaction: isoprene+OH+$NO_X$, isoprene+$NO_3$ | (Jacobs et al., 2014; Xiong et al., 2015) |
| $C_4H_7NO_5I^-$ | 275.94 | MVKN/ MACRN | 2nd-genetration organic nitrates from oxidation of IHN in the presence of $NO_X$ | (Fisher et al., 2016; Paulot et al., 2009) |
| $C_5H_9NO_5I^-$ | 289.95 | C5 nitrooxy hydroperoxide, C5 nitrooxy hydroxyepoxide, C5 dihydroxy nitrate | isoprene+$NO_3$, isoprene+OH+$NO_X$ | (Ng et al., 2017; Schwantes et al., 2015; Wennberg et al., 2018) |
| $C_8H_{12}O_4I^-$ | 298.98 | Dicarboxylic and oxocarboxylic acids like norpinic acid, terpenylic acid | Monoterpenes+OH, monoterpenes $O_3$ | (Fang et al., 2017; Mutzel et al., 2016; Yasmeen et al., 2011) |
| $C_9H_{14}O_4I^-$ | 312.99 | Dicarboxylic and oxocarboxylic acids like pinic acid, homoterpenylic acid, caric acid | Monoterpenes+OH, monoterpenes $O_3$ | (Fang et al., 2017; Mutzel et al., 2016; Yasmeen et al., 2011) |
| $C_{10}H_{16}O_3I^-$ | 311.02 | Oxocarboxylic acids like | Monoterpenes+OH, monoterpenes $O_3$ | (Fang et al., 2017; Glasius et al., |

| | | | | |
|---|---|---|---|---|
| | | pinonic acid, caronic acid | | 2000; Yasmeen et al., 2011) |
| $C_8H_{13}NO_6I^-$ | 345.98 | Organic nitrates from monoterpenes | Monoterpenes+OH+$NO_X$, monoterpenes +$NO_3$ | (Lee et al., 2016; Nah et al., 2016) |
| $C_8H_{11}NO_7I^-$ | 359.96 | Organic nitrates from monoterpenes | Monoterpenes+OH+$NO_X$, monoterpenes $O_3$+$NO_3$ | (Carslaw, 2013; Lee et al., 2016) |
| $C_{10}H_{15}NO_6I^-$ | 372.00 | Organic nitrates from monoterpenes, peroxyacetyl nitrate from pinonaldehyde | Monoterpenes+OH+$NO_X$, monoterpenes $O_3$+$NO_3$ | (Boyd et al., 2015; Massoli et al., 2018; Schwantes et al., 2020) |
| $HSO_4^-$ | 96.96 | Sulfuric acid | Oxidation of $SO_2$ etc. | (Le Breton et al., 2018b) |
| $SO_3I^-$ | 206.86 | Sulfur trioxide, Fragment of organosulfates | Oxidation of $SO_2$, decomposition of organosulfates | (Surratt et al., 2007) |
| $C_2H_3SO_6^-$ | 154.96 | Glycolic acid sulfate | Aqueous reaction of glycolic acid and sulfuric acid | (Galloway et al., 2009; Huang et al., 2018) |
| $CH_3SO_3^-$ | 94.98 | Methanesulfonic acid | Oxidation of dimethyl sulfide | (Chen and Finlayson-Pitts, 2017; Gondwe et al., 2003) |
| $N_2O_5I^-$ | 234.89 | Dinitrogen pentoxide | $NO_3$ + $NO_2$ + M | (Le Breton et al., 2018a; Wang et al., 2016) |
| $ClNO_2I^-$ | 207.87 | Nitryl chloride | $N_2O_5$ (g) + $Cl^-$ (aq) | (Le Breton et al., 2018a; Wang et al., 2016) |

| | | | | |
|---|---|---|---|---|
| $ClNO_3I^-$ | 223.86 | Chlorine nitrate | ClO + $NO_2$ + M | (Liu et al., 2017; Sander and Crutzen, 1996) |
| $Cl_2I^-$ | 196.84 | Chlorine | Heterogeneous reactions of $Cl^-$ and reactive chlorine like HOCl, $ClNO_2$ etc. | (Le Breton et al., 2018a; Liu et al., 2017; Wang et al., 2019) |
| $HNO_3I^-$ | 189.90 | Nitric acid | $NO_X$ + OH, hydrolysis of organic nitrates and $N_2O_5$ | (Fisher et al., 2016; Wang et al., 2016) |

1289

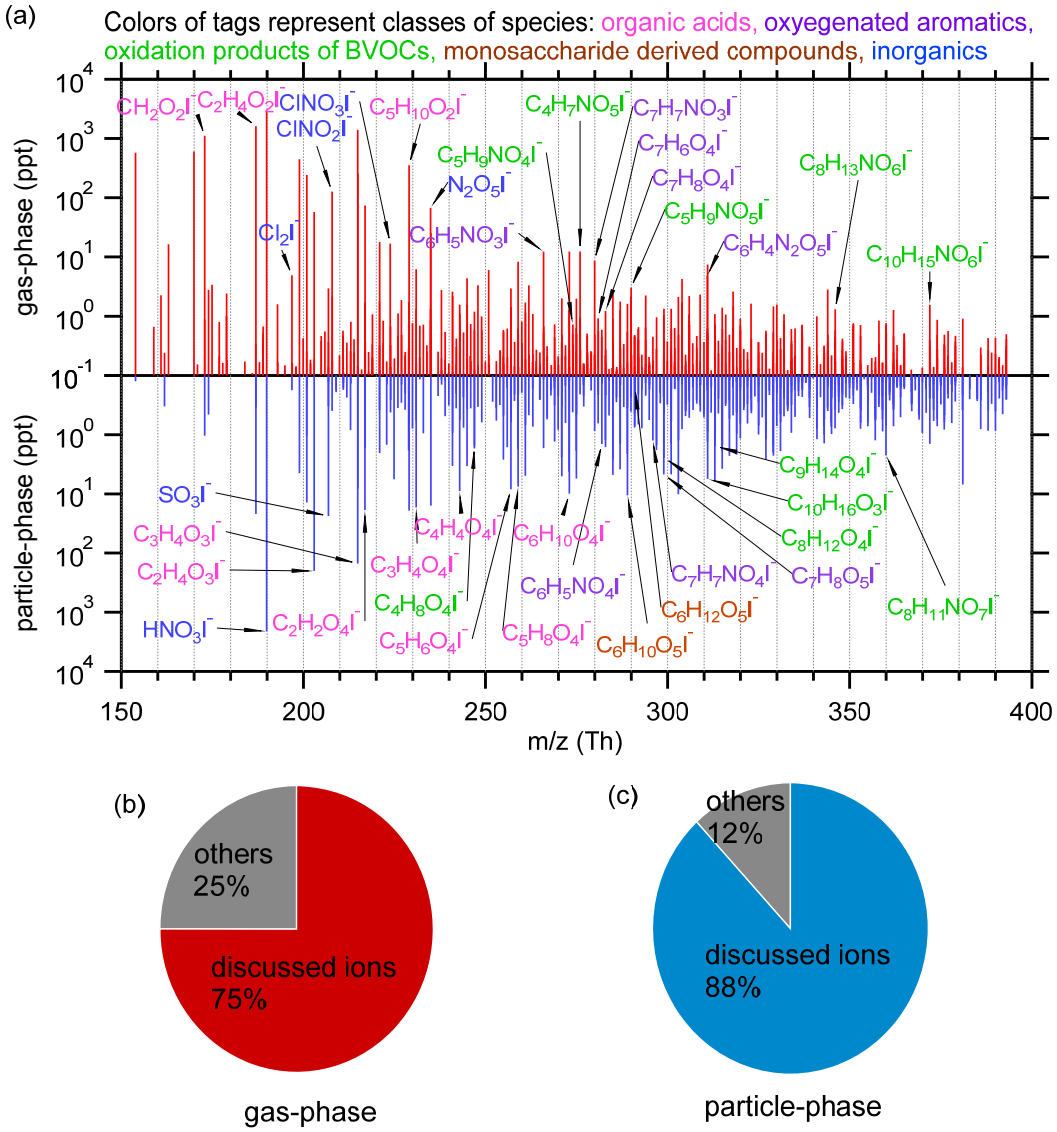


**Figure 1.** (a) Mass spectra of iodide charged ion within m/z 150-400 Th in gas-phase (red) and particle-phase (blue), respectively. (b and c) The fractions of I-adduct ions discussed in the main text (Table 1) in the total ion signals for I-adduct ions measured in gas-phase (b) and particle-phase (c), respectively.

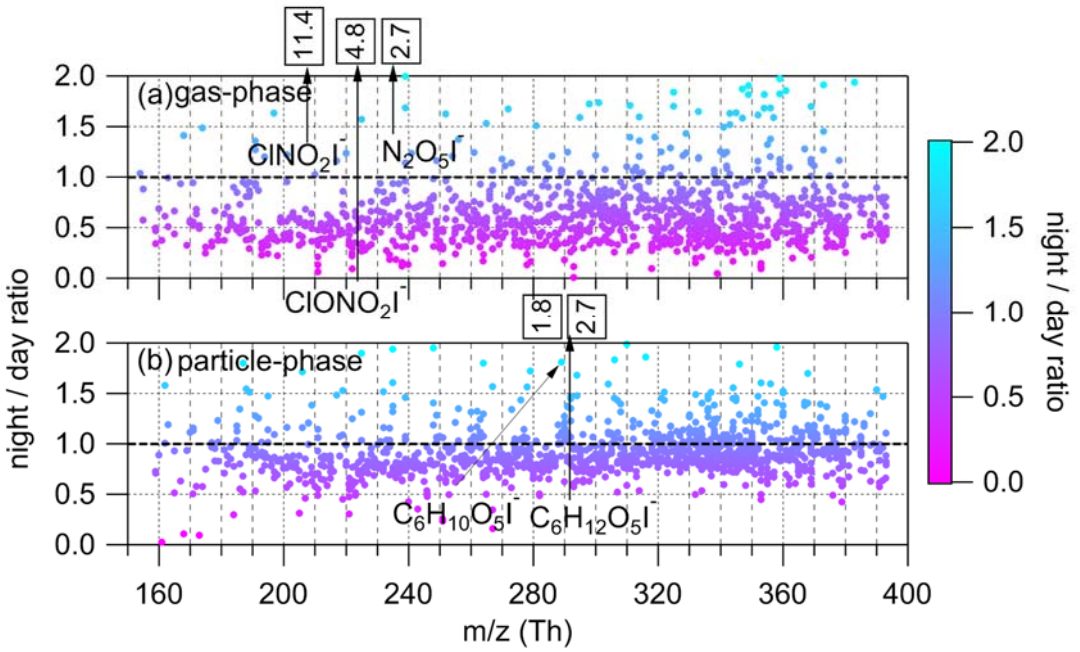


**Figure 2.** The ratios of concentrations at night (10 pm - 6 am) to concentrations during the day (10 am - 6 pm) for ions ranging from 150 to 400 Th in gas-phase (a) and particle-phase (b). The range of y-axis is set between 0 and 2 for clarity, although the ratios of some compounds are larger than 2. The numbers in boxes indicate the night/day ratios of tagged ions that exceed the y-axis ranges.

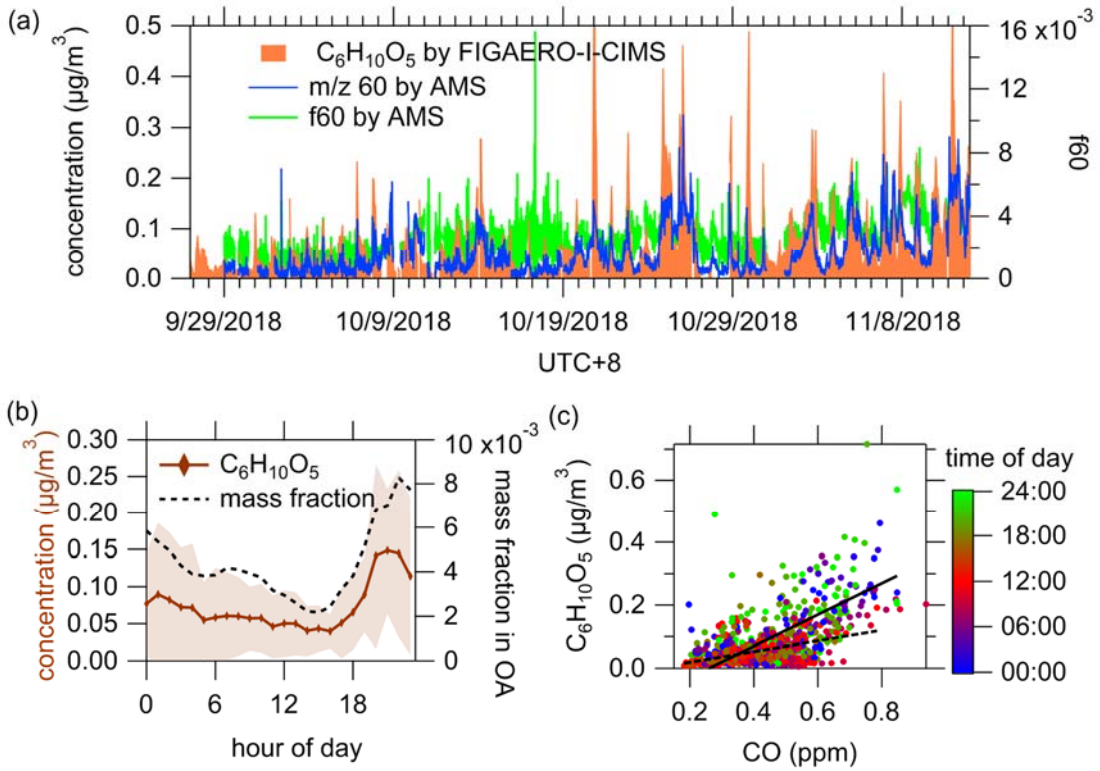


**Figure 3.** (a) Time series of particulate $C_6H_{10}O_5$ measured by FIGAERO-I-CIMS, m/z 60 fragment and f60 measured by AMS. Background f60=0.3% and background m/z 60=0.3%×OA were subtracted from f60 and m/z 60 (Cubison et al., 2011; Hu et al., 2016). (b) Diurnal variations of particulate $C_6H_{10}O_5$ and its mass fraction in OA. (c) Correlation between CO and particulate $C_6H_{10}O_5$. The dash and solid lines indicate the ratios during daytime (10 am - 6 pm, 0.17±0.02 μg·m$^{-3}$/ppm) and nighttime (10 pm - 6 am, 0.50±0.03 μg·m$^{-3}$/ppm), respectively.

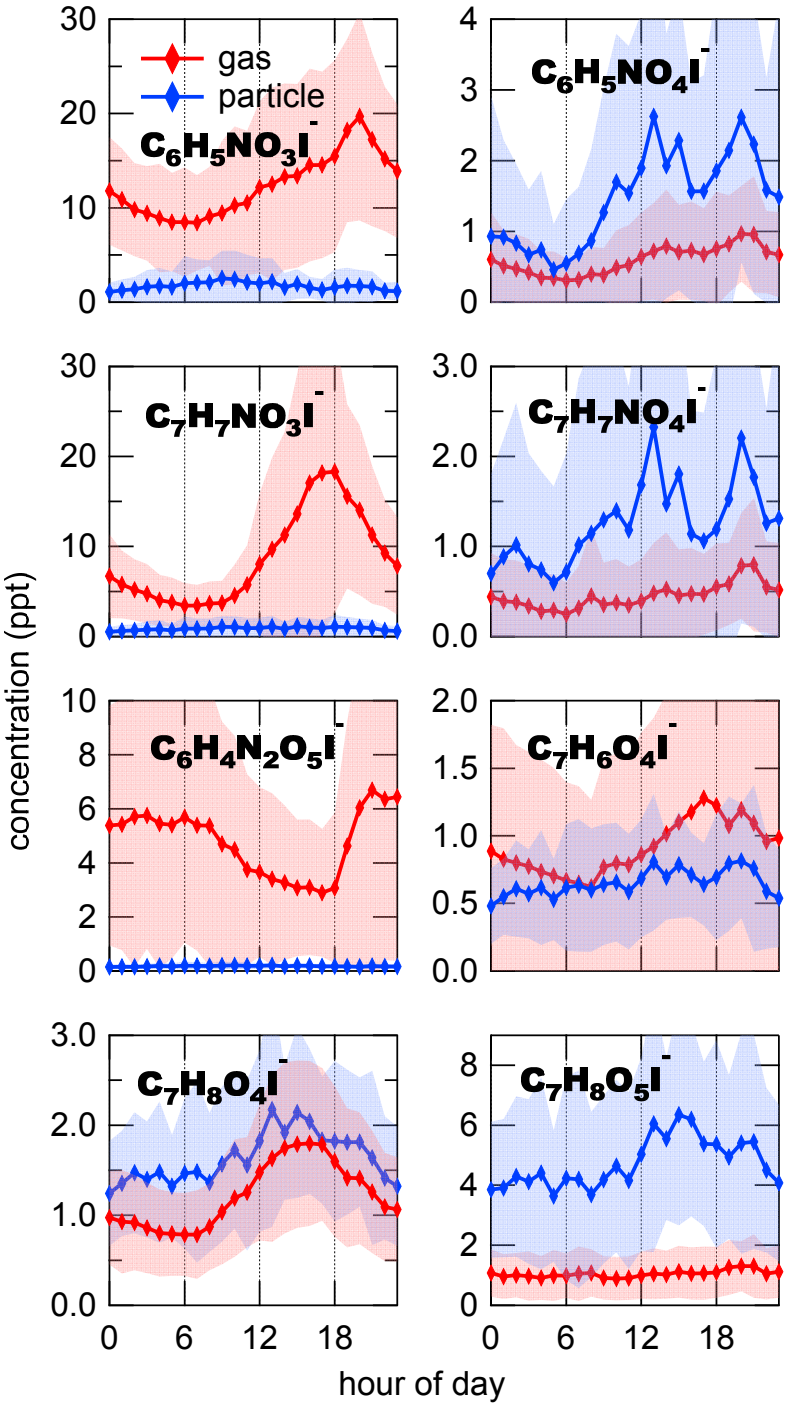


**Figure 4.** Diurnal variations of oxidized aromatics including nitro-phenols ($C_6H_5NO_3I^-$), nitro-benzenediols ($C_6H_5NO_4I^-$), methyl nitro-phenols ($C_7H_7NO_3I^-$), methyl nitro-benzenediols ($C_7H_7NO_4I^-$), dinitro-phenols ($C_6H_4N_2O_5I^-$), dihydroxy methyl benzoquinone ($C_7H_6O_4I^-$), tetrahydroxy toluene ($C_7H_8O_4I^-$), pentahydroxy toluene and fragments of C9 aromatics ($C_7H_8O_5I^-$). The shaded areas indicate one standard deviation.

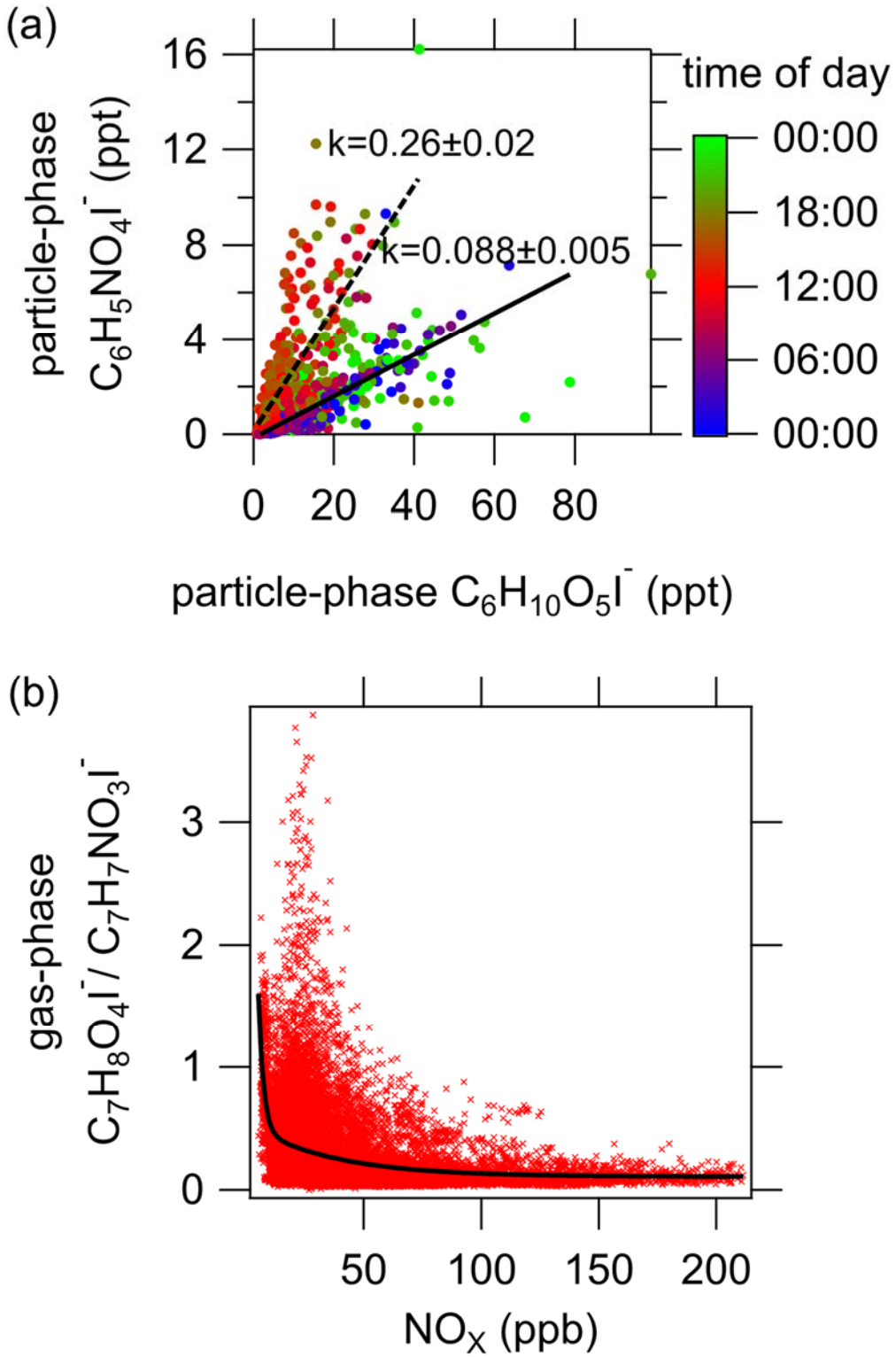


1318

1319 **Figure 5.** (a) Correlation between particle-phase $C_6H_5NO_4I^-$ and $C_6H_{10}O_5I^-$. The

1320 data points are color-coded using the time of the day. Solid and dash lines represent the

1321 slopes during the nighttime and daytime, respectively. (b) Relative concentration of

1322 $C_7H_8O_4I^-$ and $C_7H_7NO_3I^-$ in the gas phase as a function of NOx concentration. The
1323 black line is the fitted curve using a double exponential function.

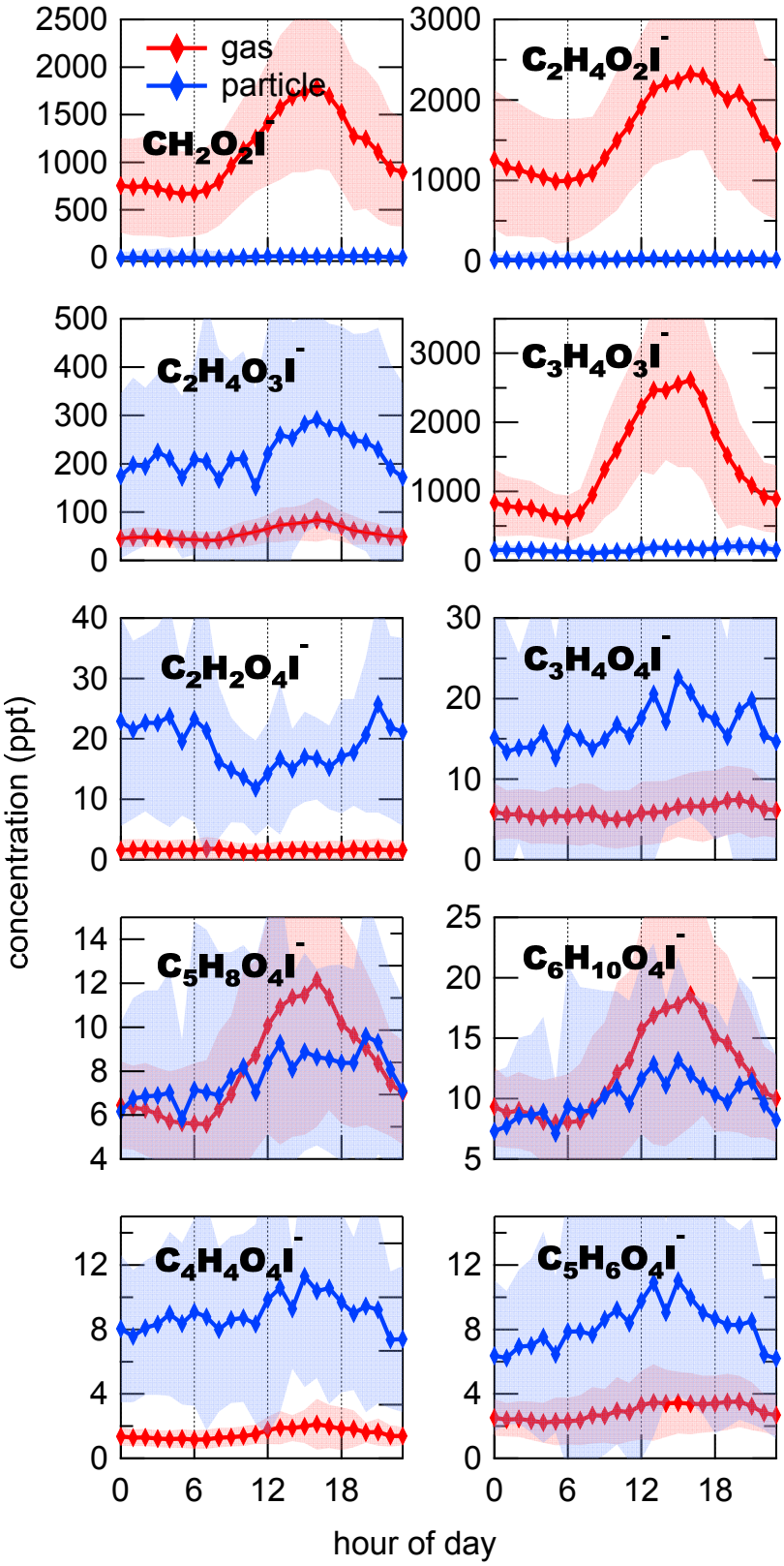


**Figure 6.** Diurnal variations of organic acids in the gas phase (red) and particle phase (blue). The shaded area indicates one standard deviation.

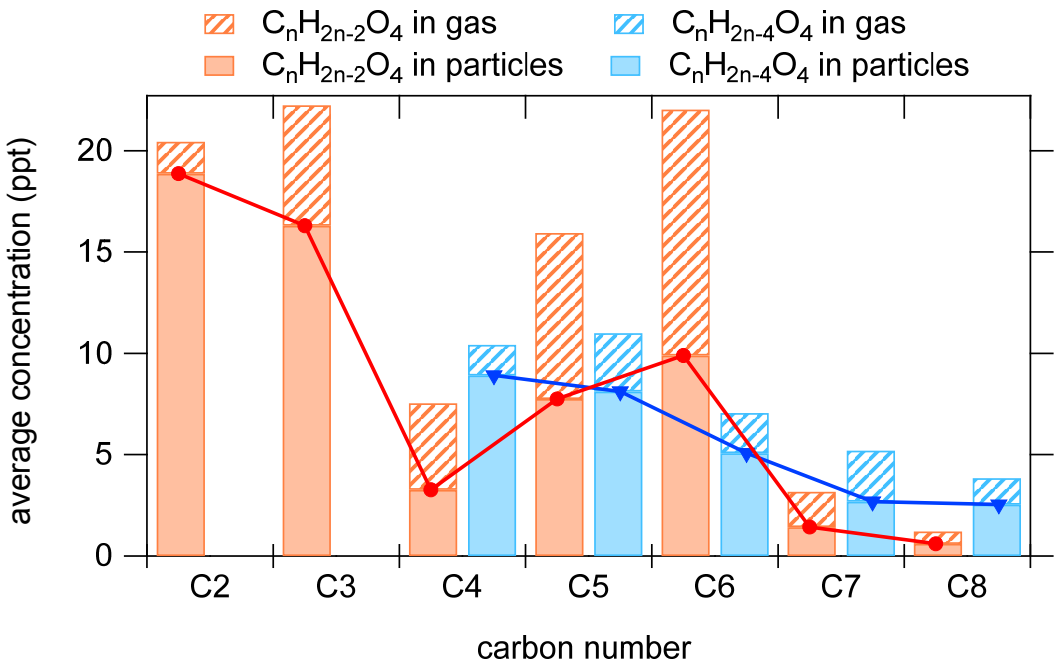


1327

1328 **Figure 7.** Average concentrations of compounds with the formulas of $C_nH_{2n-2}O_4$

1329 and $C_nH_{2n-4}O_4$.

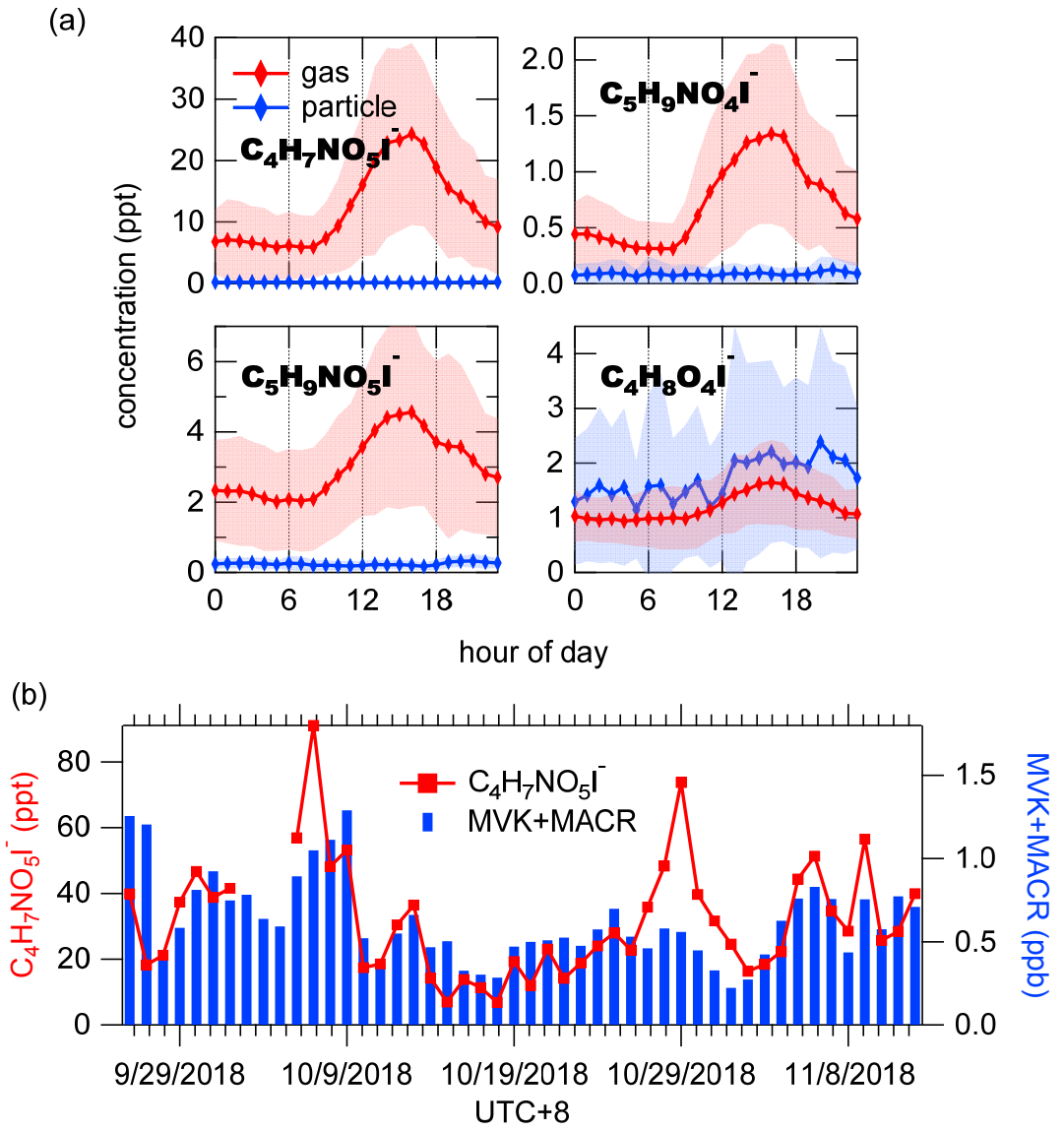


**Figure 8.** (a) Diurnal variations of isoprene oxidation products in the gas phase (red) and particle phase (blue). The shaded area indicates one standard deviation. (b) Time series of daily maximum concentrations of gaseous $C_4H_7NO_5I^-$ and MVK+MACR ($C_4H_6OH^+$, m/z 71.05) measured by PTR-ToF-MS.

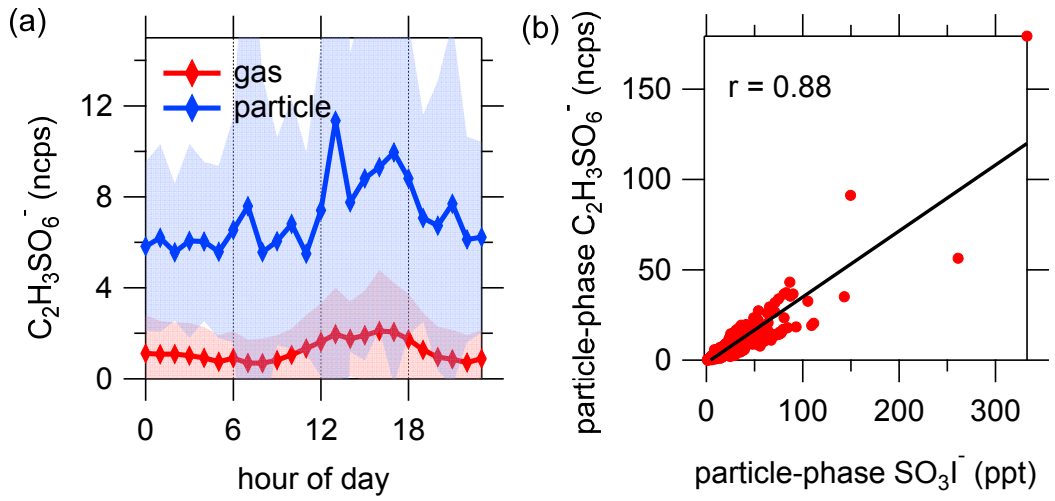


1335

1336 **Figure 9.** (a) Diurnal variation of $C_2H_3SO_6^-$. The shaded areas indicate one standard

1337 deviation. (b) Correlation between particle-phase $C_2H_3SO_6^-$ and $SO_3I^-$.

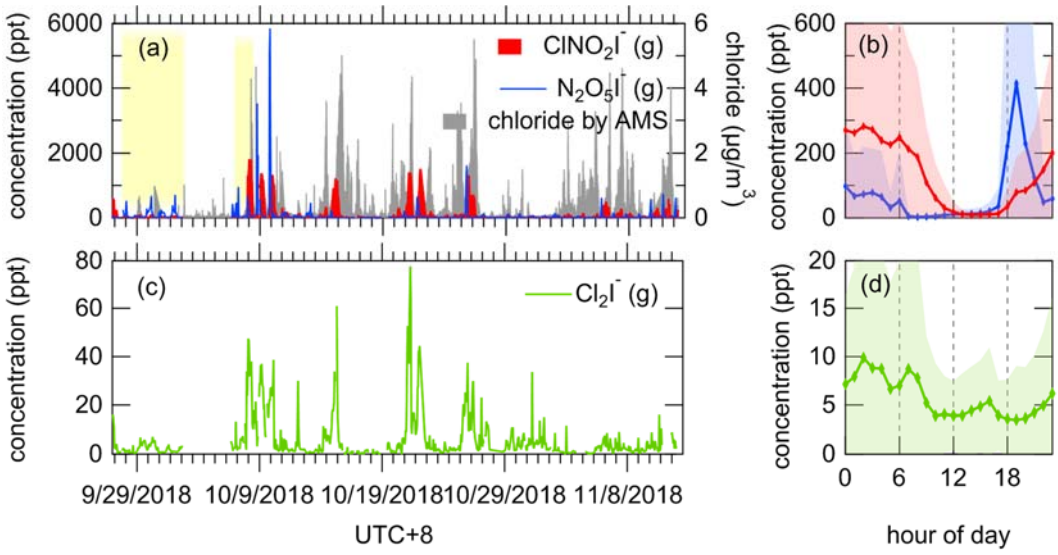


**Figure 10.** Time series and diurnal variations of humidity-corrected concentrations of $N_2O_5$ and $ClNO_2$ (a, b) and $Cl_2$ (c, d). The tinted background indicates the days with high concentrations of $N_2O_5$ but low concentrations of $ClNO_2$. The shaded areas indicate one standard deviation.

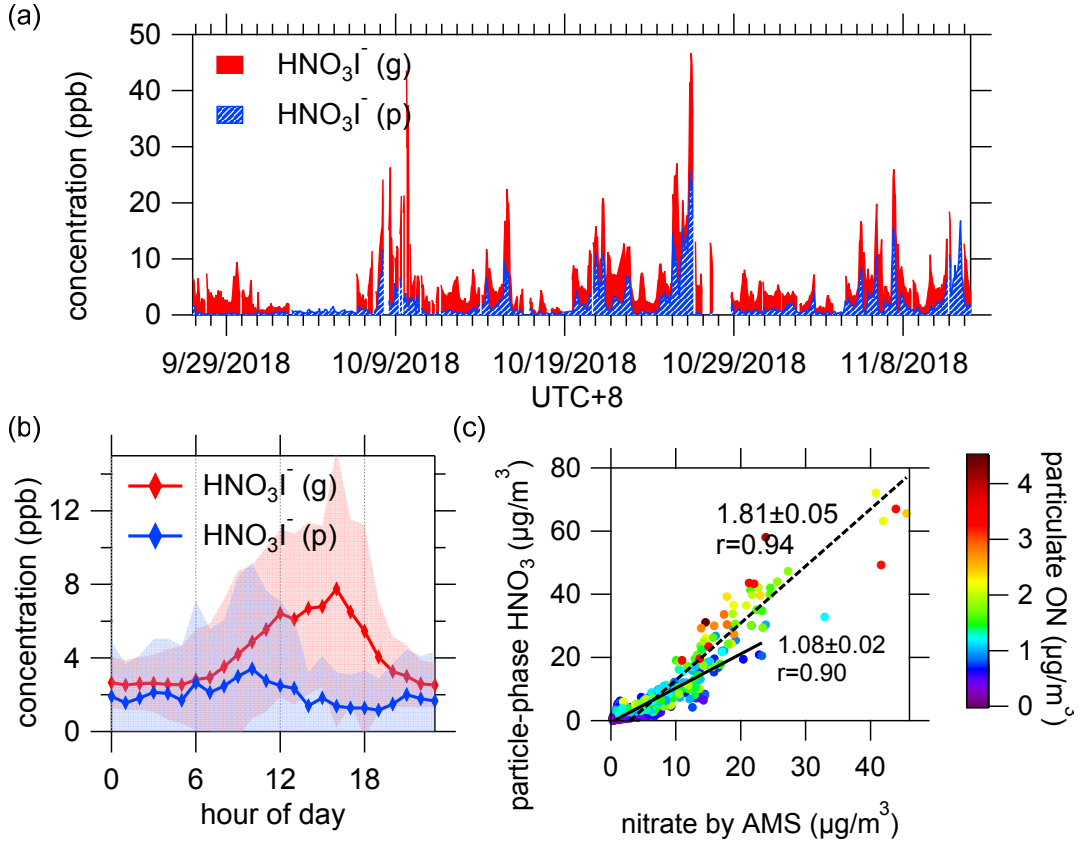


**Figure 11.** (a) Time series of humidity-corrected $HNO_3I^-$ in both phases. (b) Diurnal variation of humidity-corrected $HNO_3I^-$. The shaded areas indicate one standard deviation. (c) Comparison of particle-phase $HNO_3I^-$ and nitrate measured by AMS. The color scale denotes particulate N-containing organic compounds measured by FIGAERO-I-CIMS (pON). The solid and dash lines show the fitted results for the dataset of pON less than 1 μg/m$^3$ and more than 1 μg/m$^3$, respectively. The concentration of gaseous $HNO_3I^-$ shown here only included the last 5-minute of every gas-phase working mode, as high level of $HNO_3$ came out of aerosol which then passed through the CIMS in a short time during particle analysis and a substantial amount would subsequently accumulate on the inner surfaces, leading to a persistent carried over signal that was long enough to disturb the next gas measurement cycle (Palm et al., 2019).

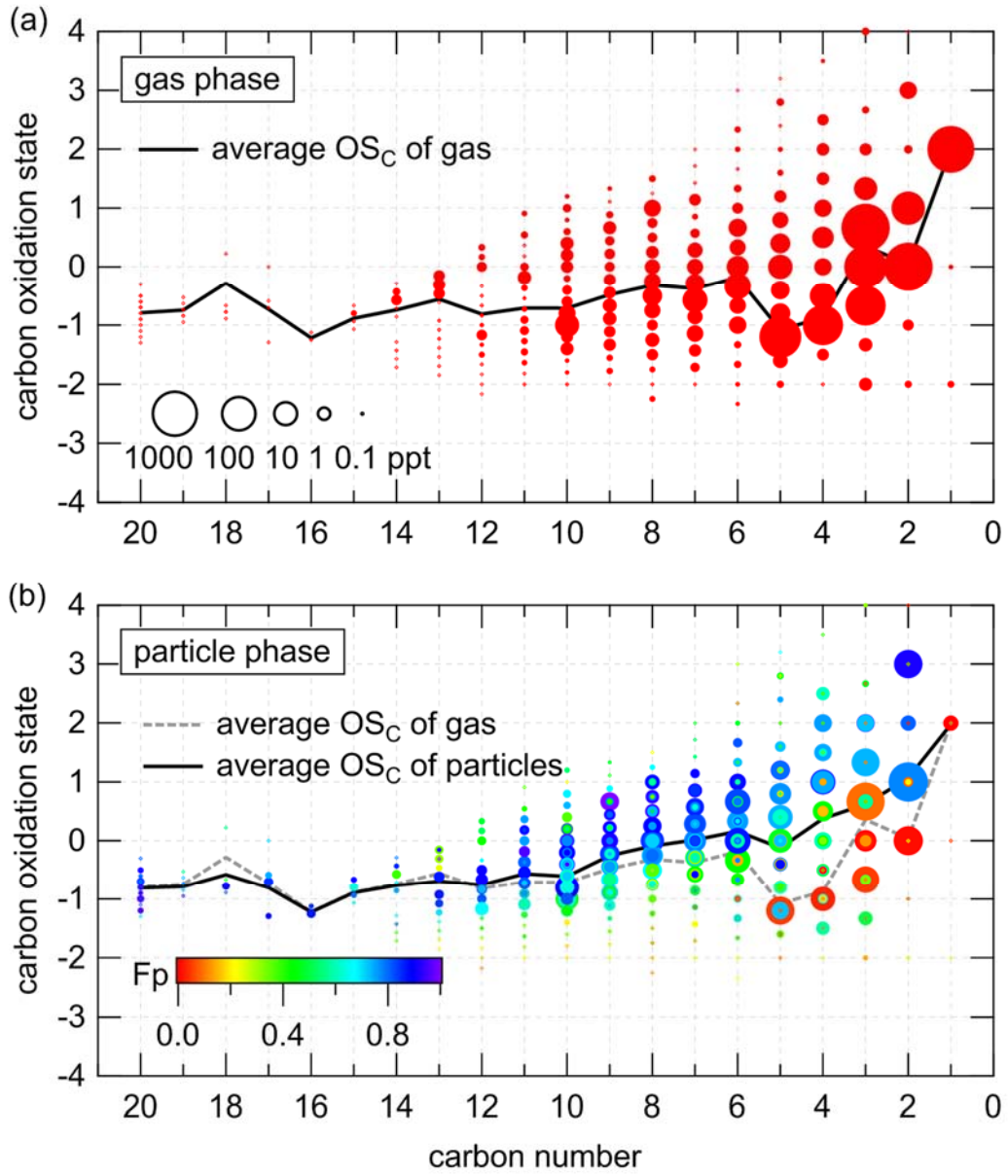


**Figure 12.** $\overline{OS_C} - n_C$ spaces for $C_xH_yO_z$ and $C_xH_yN_{1,2}O_z$ compounds in gas-phase (a) and particle-phase (b). The diameters of circles are proportional to the logarithmic average concentrations. The black lines are the average $\overline{OS_C}$ of each carbon number for compounds in gas-phase and particle-phase, respectively. The compounds in Fig. (b) are color-coded by their fractions in particles.

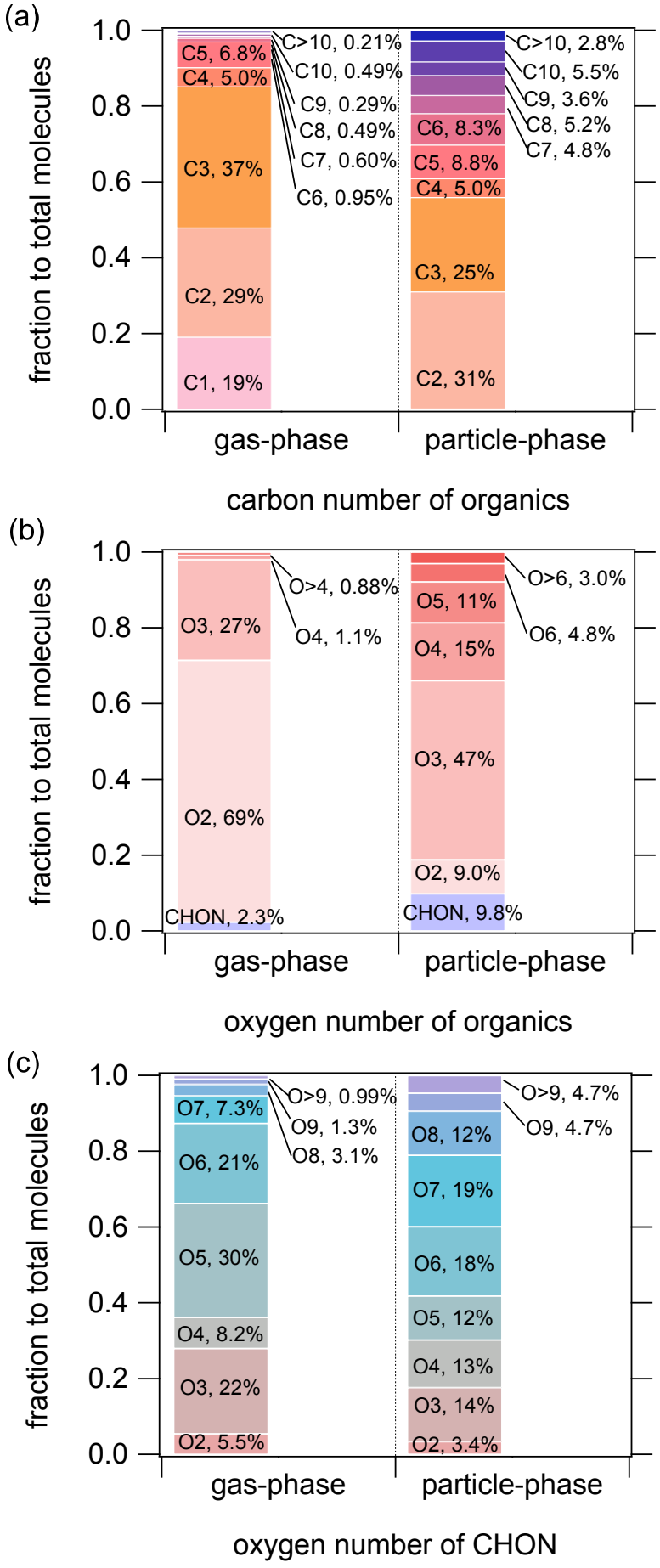
(a)
fraction to total molecules
1.0
0.8
0.6
0.4
0.2
0.0
C5, 6.8%
C4, 5.0%
C3, 37%
C2, 29%
C1, 19%
C>10, 0.21%
C10, 0.49%
C9, 0.29%
C8, 0.49%
C7, 0.60%
C6, 0.95%
C>10, 2.8%
C10, 5.5%
C9, 3.6%
C8, 5.2%
C7, 4.8%
C6, 8.3%
C5, 8.8%
C4, 5.0%
C3, 25%
C2, 31%
gas-phase
particle-phase
carbon number of organics
(b)
fraction to total molecules
1.0
0.8
0.6
0.4
0.2
0.0
O3, 27%
O2, 69%
CHON, 2.3%
O>4, 0.88%
O4, 1.1%
O>6, 3.0%
O5, 11%
O4, 15%
O3, 47%
O2, 9.0%
CHON, 9.8%
O6, 4.8%
gas-phase
particle-phase
oxygen number of organics
(c)
fraction to total molecules
1.0
0.8
0.6
0.4
0.2
0.0
O7, 7.3%
O6, 21%
O5, 30%
O4, 8.2%
O3, 22%
O2, 5.5%
O>9, 0.99%
O9, 1.3%
O8, 3.1%
O>9, 4.7%
O8, 12%
O7, 19%
O6, 18%
O5, 12%
O4, 13%
O3, 14%
O2, 3.4%
O9, 4.7%
gas-phase
particle-phase
oxygen number of CHON

1363

**Figure 13.** Carbon number distribution (a) and oxygen number distribution of total $C_xH_yO_z$ and $C_xH_yN_{1,2}O_z$ compounds (b), and oxygen number distribution of $C_xH_yN_{1,2}O_z$ compounds (c).

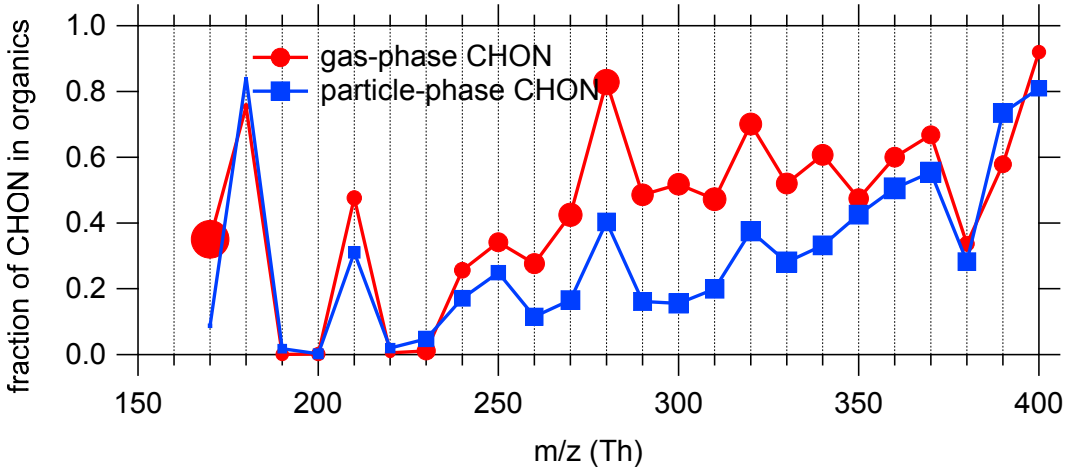


**Figure 14.** The average fractions of CHON to total organic compounds (CHO + CHON + CHOS + CHONS) of every 10 Th in both phases. See Fig. S16 for the overall distribution of the contributions of species classes to the total concentrations. Marker sizes indicate the total concentration level in each m/z bin. High ambient concentration of HNCO resulted in the large marker around m/z 170 in the gas phase (Wang et al., 2020d).

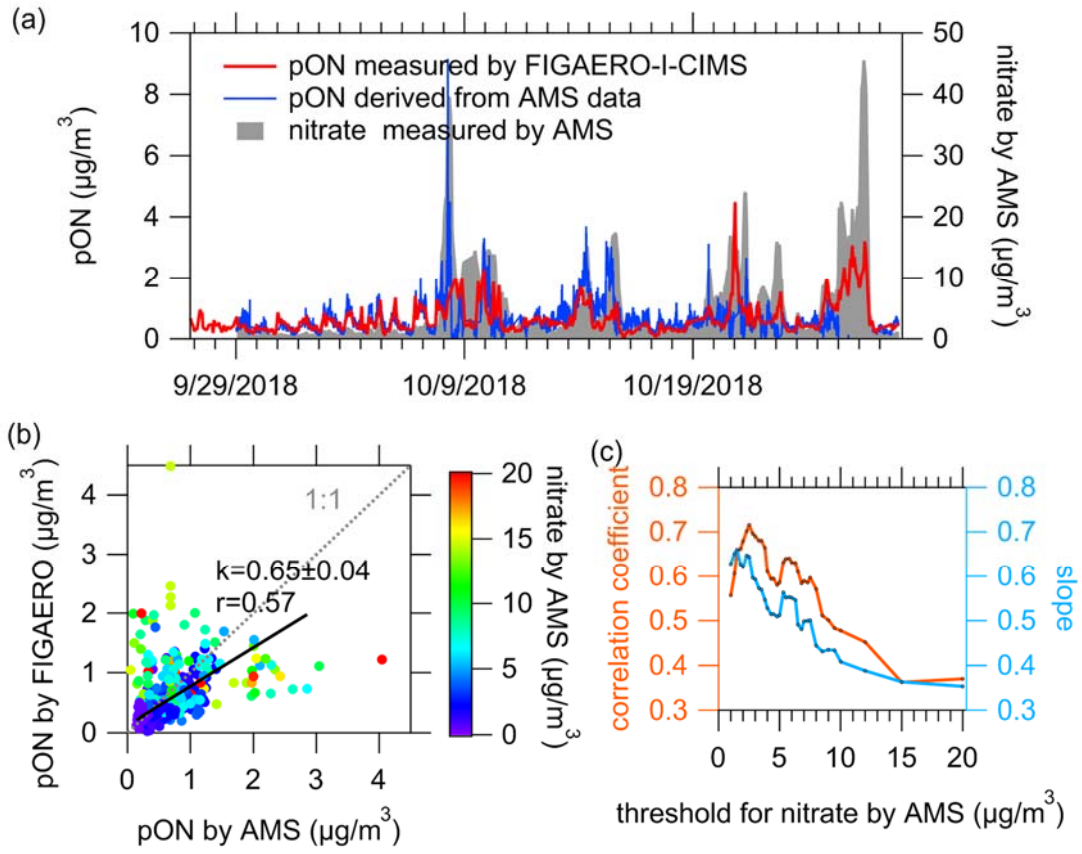


**Figure 15.** (a) Time series of particulate N-containing organic compounds measured by FIGAERO-I-CIMS (pON by FIGAERO), particulate organic nitrates derived from AMS data (pON by AMS) as well as particulate inorganic nitrate. (b) Comparison of pON by FIGAERO and pON by AMS, color-coded by the concentrations of particulate inorganic nitrate measured by AMS. The black line presents the linear fit for nitrate by AMS below 8 μg/m$^3$. (c) The determined slopes and correlation coefficients between pON by FIGAERO versus pON by AMS by filtering the data below different thresholds of particulate inorganic nitrate measured by AMS.

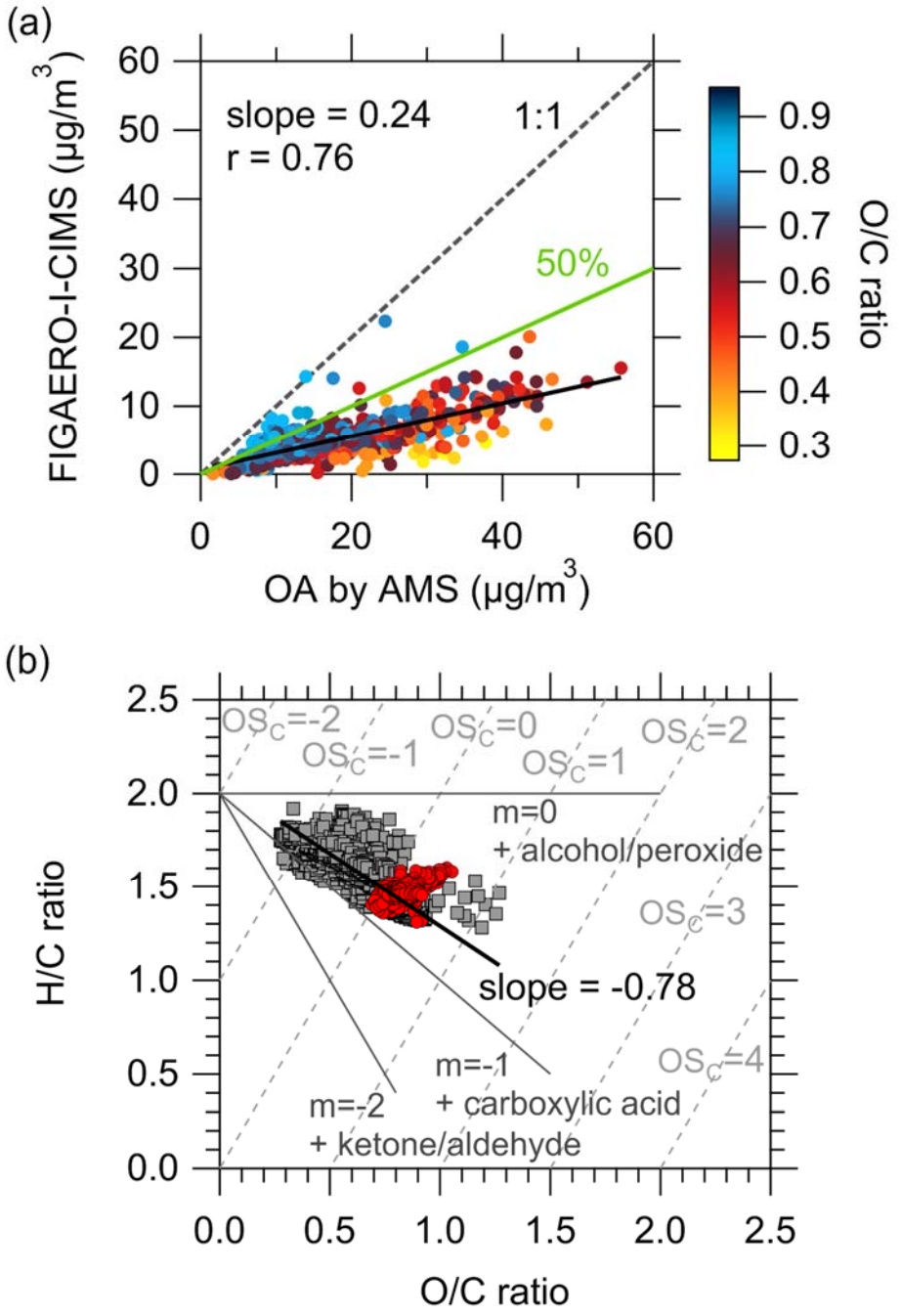


**Figure 16.** (a) Comparison of particulate organic compounds measured by the FIGAERO-I-CIMS and AMS, color-coded by O/C ratios measured by AMS. The black line is the slope which represents the fraction of OA explained by the measurements of FIGAERO-I-CIMS. The green line shows the results from previous work which were ~50% (Lopez-Hilfiker et al., 2016; Stark et al., 2017). (b) Van Krevelen diagrams for organic aerosol derived from AMS data (gray squares) and FIGAERO-I-CIMS data (red circles). Black line is the slope of AMS data. Gray dotted lines are estimated carbon oxidation state.